Multitemperature slip boundary conditions: Closed theoretical formulation for non-equilibrium reacting gas flows

L. Shakurova[1,2] and E. Kustova[1,2]
[1)]*Saint-Petersburg State University, Department of Mathematics and Mechanics, 7/9 Universitetskaya nab., St. Petersburg, 199034 Russia*
[2)]*Federal Research Center "Computer Science and Control" of the Russian Academy of Sciences, 44-2 ul. Vavilova, Moscow, 119333 Russia*

(*Electronic mail: liya.shakurova@spbu.ru)

(Dated: 20 September 2025)

This study presents a self-consistent framework for deriving slip boundary conditions within multitemperature modeling of non-equilibrium reacting gas mixtures flows. The framework is based on a previously developed method using the kinetic boundary condition, extended to account correctly for particles loss due to adsorption, desorption, and surface chemical reactions. Relations for velocity slip, translational-rotational temperature jump, and vibrational temperature jumps are derived without additional phenomenological assumptions under specular-diffusive scattering model. These conditions simultaneously account for gas–surface scattering effects and heterogeneous processes, including rotational and vibrational relaxation. A solver is developed to compute the resulting nonlinear system, with recommendations provided for integration into fluid-dynamic codes. Parametric studies of temperature jumps, relative changes in mixture composition, and surface heat flux are carried out by varying the recombination probability on the surface, accommodation coefficient, wall temperature, and Knudsen number. It is demonstrated that vibrational temperature jumps are critical for predicting near-wall flow properties, and that rotational relaxation significantly affects the temperature jump, especially when there is a large temperature difference between the gas phase and the wall. The framework enables accurate modeling of non-equilibrium gas flows near surfaces in both continuum and slip-flow regimes.

I. INTRODUCTION

Modeling of non-equilibrium reacting gas flows remains a focus of scientific research in recent decades[1–6] due to their importance for high-speed aerodynamics, aerospace applications, low-temperature plasma science and technology, environmental sciences, and microelectromechanical systems. Under non-equilibrium conditions, fluid dynamics and transport phenomena are strongly coupled to multiple physical and chemical processes such as internal energy exchange and chemical reactions, both in the gas phase and on the solid surface. Development and implementation of accurate mathematical models for such flows is one of the challenges in modern non-equilibrium gas dynamics and kinetic transport theory.

Depending on physical conditions, approaches of various detail can be applied for the flow description. The kinetic approach based on direct simulation Monte Carlo (DSMC)[4,7,8], while being an excellent tool for the rarefied and transient flows, becomes computationally expensive with decreasing Knudsen number; moreover there is a lack of reliable DSMC models for the cross sections of chemical reactions and internal energy exchange in polyatomic gases. In computational fluid dynamics (CFD), a continuum approach based on macroscopic fluid dynamic equations is applied. Fundamentals of the continuum approach based on the Chapman–Enskog method are given in Refs. 9–11. Continuum approaches are limited to low Knudsen numbers; however, taking into account non-equilibrium effects in extended sets of fluid dynamic equations expands the limits of its applicability.

The most detailed among continuum models is the state-to-state (STS) gas flow description taking into account all excited vibrational states in a mixture as pseudo species[2,12–19]. This approach provides valuable information on key relaxation mechanisms under various conditions, but is still hardly applicable for viscous flow simulations due to prohibitively expensive algorithms for the evaluation of state-resolved transport coefficients.

A good alternative providing satisfactory accuracy at a lower computational cost is the multitemperature (MT) flow model. Semi-empirical MT models[1,20,21] are easy to implement in CFD codes but they are limited by many assumptions introduced for modeling rates of coupled vibrational-chemical relaxation and transport properties. Self-consistent theoretical models of transport processes in multitemperature flows taking into account anharmonicity and accurate chemical-vibrational coupling are developed in Refs. 22 and 23 in the frame of the generalized Chapman–Enskog method; rigorous models for the MT chemical and vibrational energy production rates taking into account cross effects between the rates of non-equilibrium processes and normal mean stress are proposed in Refs. 24 and 25. Further improvement of multitemperature models is provided in Refs. 26 and 27 in the frame of a hybrid approach combining simple MT fluid dynamic equations with exact state-to-state energy and chemical production rates. Thus, in these studies, the fully self-consistent closure of MT fluid dynamic equations for viscous thermochemically non-equilibrium flows was carried out. However, no accurate models for boundary conditions obtained in the same kinetic-theory framework have been developed up to now, which prevents simulations of real viscous non-equilibrium flows near solid surfaces with different catalytic properties.

Boundary conditions (BCs) for a multitemperature set of fluid dynamic variables must capture slip effects in gas flows near surfaces, typically represented through velocity slip and temperature jump relations; non-equilibrium heterogeneous

processes, such as adsorption/desorption and surface reactions, which commonly appear in near-wall mass flux expressions; and excitation or deactivation of vibrational energy in molecular components of the mixture due to scattering by the solid surface and heterogeneous processes, which must be included in additional boundary conditions for vibrational temperatures (vibrational temperature jumps) in the MT approximation. Additionally, these BCs should account for all processes simultaneously, otherwise, the macroparameters after gas–wall interaction can be evaluated incorrectly[28]. For studies addressing the individual influence of such processes, see, e.g., Refs. 5, 21, 29–35. To our knowledge, such comprehensive conditions do not yet exist. Consequently, multitemperature modeling of non-equilibrium gas flows near solids has been performed using phenomenological or simplified theoretical models, e.g. see Refs. 36–42. Most of these models were developed for a single vibrational temperature, or even a single internal temperature[40] (the only exception being Ref. 39), and did not account for slip effects in vibrational temperature jump or for heterogeneous processes.

This work addresses this gap by developing appropriate slip boundary conditions for MT models. For this purpose, we modify a previously developed method for obtaining slip BCs based on the kinetic boundary condition[28,43,44]. In addition, we reexamine the modeling of heterogeneous reactions to correctly capture particle loss due to surface processes and include the effect of rotational relaxation in the slip BCs.

The objectives of this study are: 1) to modify and generalize the previously developed kinetic BC to take into account newly formed and desorbed particles; 2) to apply the updated kinetic BC to derive a fully closed MT flow description with slip boundary conditions, including vibrational temperature jumps; 3) to compare the obtained BCs with those previously derived within the STS approach and with other BCs for MT models; 4) to implement and assess the MT BC model; 5) to evaluate the influence of the modified kinetic BC on the modeling of gas–surface processes and to identify the limits of applicability for the simplified model proposed in earlier work; 6) to carry out a parametric study to estimate the effects of surface reaction probabilities, rotational degrees of freedom, and diffusion on the molar fractions, rotational-translational temperature, vibrational temperatures, and heat flux.

The paper is organized as follows. In Section II, we provide a closed system of governing equations for modeling gas mixture flows under the multitemperature approximation. Section III develops a method for deriving slip BCs from the kinetic boundary condition. Section IV introduces the resulting closed set of MT boundary conditions. A brief overview of their implementation in numerical codes, along with the results of a parametric study, are given in Section V. Concluding remarks are provided in Section VI. Mathematical details of the BCs derivation are given in Supplementary Material.

II. MULTITEMPERATURE MODEL FOR NON-EQUILIBRIUM GAS MIXTURE FLOWS

Before formulating the approach for deriving slip boundary conditions, we first briefly review the key features of multitemperature models.

To obtain a closed set of governing equations for non-equilibrium mixture flows within the continuum framework, we follow the generalized Chapman–Enskog method[2]. In this method, the following form of the Boltzmann equation (Wang Chang–Uhlenbeck extension of the Enskog equation) is considered:

$$\frac{\partial f_{cij}}{\partial t} + \mathbf{u}_c \cdot \nabla f_{cij} = \frac{1}{\varepsilon} J^{\mathrm{rap}}_{cij} + J^{\mathrm{sl}}_{cij}, \qquad c = 1,\ldots,L, \quad i = 0,\ldots,N_c, \quad j = 0,\ldots,N_{ci}. \tag{1}$$

Here, the distribution function $f_{cij}(\mathbf{r},\mathbf{u},t)$ is introduced for chemical species c, vibrational level i, and rotational level j; the electronic excitation is neglected; $\mathbf{r}$ denotes the spatial coordinate, $\mathbf{u}_c$ is the species c velocity, t is the time; L is the number of chemical species; N_c is the number of vibrational levels for c species; N_{ci} is the number of rotational levels of molecules c on the vibrational level i. The collision operators account for the variation of the distribution function due to rapid, J^{rap}_{cij}, and slow, J^{sl}_{cij}, processes[2]. The small parameter ε is introduced as the ratio of characteristic times of rapid and slow processes.

When rapid and slow processes are specified, the distribution function is represented as a generalized Chapman–Enskog series in terms of the small parameter. Commonly, only terms up to the first order are considered. This approach allows one to define a closed set of fluid dynamic equations, including procedures for calculating transport coefficients and expressions for the relaxation terms. The details can be found in Ref. 2.

In this work, we consider only gas mixtures composed of atoms and diatomic molecules, excluding polyatomic molecules, where energy transitions between modes must be taken into account. For these mixtures, we consider the following relation between the relaxation times:

$$\tau_{\mathrm{tr}} < \tau_{\mathrm{rot}} < \tau_{\mathrm{VV}_c} \ll \tau_{\mathrm{VV}'} \sim \tau_{\mathrm{VT}} \sim \tau_{\mathrm{react}} \sim \theta, \tag{2}$$

where τ_{tr}, τ_{rot} are the characteristic times of translational and rotational relaxation; τ_{VV}, τ_{VT}, τ_{react} are the characteristic time scales of vibrational-vibrational (VV) and vibrational-translational (VT) energy transitions, and chemical reactions; θ is the fluid dynamic time scale; τ_{VV_c} denotes the time of VV transitions between molecules of the same species, while $\tau_{\mathrm{VV}'}$ corresponds to VV transitions occurring between different molecular species. According to kinetic scaling (2), near-resonant vibrational energy exchanges between molecules of the same chemical species occur significantly faster than non-resonant transitions between different molecules, as well as transfers of vibrational energy to other modes or chemical reactions.

The chosen time scale allows one to specify the invariants of the most frequent collisions corresponding to rapid

processes. For kinetic scaling (2), these invariants are the mass, the momentum, and the total energy of c species (rotational and vibrational motions are treated as independent in this study):

$$\psi_{cij}^{(\nu)} = m_c,\ m_c\mathbf{u}_c,\ \frac{m_c u_c^2}{2} + \varepsilon_j^c + \varepsilon_i^c + \varepsilon_c,\ \nu = 1,\ldots,5; \quad (3)$$

and additional invariants of rapid processes[2]:

$$\psi_{cij}^{(\mu+5)} = a_c,\ \mu = 1,\ldots,L; \quad (4)$$

$$\psi_{cij}^{(\lambda+L+5)} = \varepsilon_i^c,\ \lambda = 1,\ldots,L_{\mathrm{m}}. \quad (5)$$

Here, m_c is the species mass; ε_j^c, ε_i^c, ε_c are the species c rotational energy on the level j, vibrational energy on the level i, and energy of formation, respectively; L_{m} is the number of molecular species; a_c is a value independent of the velocity, vibrational i and rotational j quantum numbers and depending arbitrarily on the chemical species c; usually a_c is set to 1; such a choice yields species number densities to be additional macroscopic variables governed by corresponding conservation equations. Collision invariants (5) represent the conservation of vibrational energy when molecules of the same species collide. More generally, instead of (5), another additional invariant should be considered — the total number of vibrational quanta. However, when molecular vibrations are modeled as harmonic oscillators, the vibrational energy (5) remains invariant under rapid elastic and VV$_c$ collisions between molecules of the same species. From this point on, we will consider the set of collision invariants given by (3)–(5).

The set of collision invariants allows one to determine a set of fluid dynamic variables that describe the flow within the framework of the chosen approximation. For the MT approach based on kinetic scaling (2), the set of macroscopic parameters includes the number densities of gas species $n_c(\mathbf{r},t)$, gas velocity $\mathbf{v}(\mathbf{r},t)$, gas translational-rotational temperature $T(\mathbf{r},t)$, and additional vibrational temperatures for molecular species $T_c^{\mathrm{v}}(\mathbf{r},t)$.

The system of transport equations is obtained by multiplying the Boltzmann equation (1) by the collision invariants of the most frequent collisions, followed by integration over the entire velocity space, summation over all species, and summation over all internal energy states when considering molecular species:

$$\frac{\partial \mathbf{Q}}{\partial t} + \frac{\partial \mathbf{F}_x}{\partial x} + \frac{\partial \mathbf{F}_y}{\partial y} + \frac{\partial \mathbf{F}_z}{\partial z} + \frac{\partial \mathbf{F}_x^v}{\partial x} + \frac{\partial \mathbf{F}_y^v}{\partial y} + \frac{\partial \mathbf{F}_z^v}{\partial z} = \mathbf{H}. \quad (6)$$

The vector of conservative variables $\mathbf{Q}$ and the vectors of convective fluxes $\mathbf{F}_q$ are defined as follows:

$$\mathbf{Q} = \begin{pmatrix} \rho \\ \rho y_c \\ \rho v_x \\ \rho v_y \\ \rho v_z \\ \rho E \\ \rho y_c E_{\mathrm{vibr},c} \end{pmatrix},\ \mathbf{F}_x = \begin{pmatrix} \rho v_x \\ \rho y_c v_x \\ \rho v_x v_x + p \\ \rho v_x v_y \\ \rho v_x v_z \\ (\rho E + p) v_x \\ \rho y_c E_{\mathrm{vibr},c} v_x \end{pmatrix},\ \mathbf{F}_y = \begin{pmatrix} \rho v_y \\ \rho y_c v_y \\ \rho v_y v_x \\ \rho v_y v_y + p \\ \rho v_y v_z \\ (\rho E + p) v_y \\ \rho y_c E_{\mathrm{vibr},c} v_y \end{pmatrix},\ \mathbf{F}_z = \begin{pmatrix} \rho v_z \\ \rho y_c v_z \\ \rho v_z v_x \\ \rho v_z v_y \\ \rho v_z v_z + p \\ (\rho E + p) v_z \\ \rho y_c E_{\mathrm{vibr},c} v_z \end{pmatrix}. \quad (7)$$

The viscous flux vectors $\mathbf{F}_q^v$ and the source $\mathbf{H}$ term are written in the following form:

$$\mathbf{F}_x^v = \begin{pmatrix} 0 \\ J_{c,x} \\ \tau_{xx} \\ \tau_{xy} \\ \tau_{xz} \\ \mathbf{v}\cdot\boldsymbol{\tau}_x + q_x \\ q_{x,c}^{\mathrm{vibr}} \end{pmatrix},\ \mathbf{F}_y^v = \begin{pmatrix} 0 \\ J_{c,y} \\ \tau_{yx} \\ \tau_{yy} \\ \tau_{yz} \\ \mathbf{v}\cdot\boldsymbol{\tau}_y + q_y \\ q_{y,c}^{\mathrm{vibr}} \end{pmatrix},\ \mathbf{F}_z^v = \begin{pmatrix} 0 \\ J_{c,z} \\ \tau_{zx} \\ \tau_{zy} \\ \tau_{zz} \\ \mathbf{v}\cdot\boldsymbol{\tau}_z + q_z \\ q_{z,c}^{\mathrm{vibr}} \end{pmatrix},\ \mathbf{H} = \begin{pmatrix} 0 \\ R_c^{\mathrm{react}} \\ 0 \\ 0 \\ 0 \\ 0 \\ R_c^{\mathrm{vibr}} \end{pmatrix}. \quad (8)$$

Here, ρ is the mixture density, v_s are the velocity $\mathbf{v}$ components, y_c is the species c mass fraction ($y_c = \rho_c/\rho$, ρ_c is the species c density), p is the gas pressure ($p = \rho RT/M_{\mathrm{mix}}$, M_{mix} is the mixture molar mass), R_c^{react} is the chemical production term, and R_c^{vibr} is the vibrational energy production term taking into account VT, VV' energy transitions, and chemical-vibrational coupling[2]. The total energy of the mixture (E) is the sum of the kinetic energy and the internal energy (U):

$$E = \frac{1}{2}(v_x^2 + v_y^2 + v_z^2) + U. \quad (9)$$

Internal energy is defined as the sum of translational ($E_{\mathrm{tr}} = \sum_c y_c E_{\mathrm{tr},c}$), rotational ($E_{\mathrm{rot}} = \sum_c y_c E_{\mathrm{rot},c}$), vibrational ($E_{\mathrm{vibr}} = \sum_c y_c E_{\mathrm{vibr},c}$), and formation energies ($E_{\mathrm{f}} = \sum_c y_c E_{\mathrm{f},c}$) of the

mixture per unit mass:

$$U = \sum_c y_c \left(E_{\mathrm{tr},c} + E_{\mathrm{rot},c} + E_{\mathrm{vibr},c} + E_{\mathrm{f},c}\right) = \sum_c y_c h_c - \frac{p}{\rho}$$
$$= \sum_c y_c \left(\frac{3}{2}\frac{kT}{m_c} + \frac{kT}{m_c} + \frac{\sum_i \varepsilon_i^c \exp\left(-\frac{\varepsilon_i^c}{kT_c^{\mathrm{v}}}\right)}{m_c Z_c^{\mathrm{vibr}}(T_c^{\mathrm{v}})} + E_{\mathrm{f},c} \right), \quad (10)$$

where h_c is the specific enthalpy of species c, k is the Boltzmann constant, and the vibrational partition function is calculated as follows:

$$Z_c^{\mathrm{vibr}}(T_c^{\mathrm{v}}) = \sum_i \exp\left(-\frac{\varepsilon_i^c}{kT_c^{\mathrm{v}}}\right). \quad (11)$$

In expression (10), we assume that rotational motion is described on the basis of the rigid rotator model.

The transport terms under the multitemperature mixture flow description (6)–(8) include the mass flux of species c, $\mathbf{J}_c$, written in terms of the diffusion velocity $\mathbf{V}_c$ of species c, $\mathbf{J}_c = \rho_c \mathbf{V}_c$; the stress tensor, $\mathbf{P} = p\mathbf{I} + \boldsymbol{\tau}$, which includes the viscous stress $\boldsymbol{\tau}$; the total heat flux vector, $\mathbf{q}$; and vibrational energy fluxes, $\mathbf{q}_c^{\mathrm{vibr}}$. In the first-order approximation of the modified Chapman–Enskog method, the transport terms can be written in the following form[2]:

$$\mathbf{V}_c = -\sum_d D_{cd}\mathbf{d}_d - D_{Tc}\nabla \ln T, \quad (12)$$

$$\boldsymbol{\tau} = -\left(\zeta \nabla\cdot\mathbf{v} + p_{\mathrm{rel}}\right)\mathbf{I} - 2\eta\left(\frac{1}{2}\left(\nabla\mathbf{v} + \nabla\mathbf{v}^T\right) - \frac{1}{3}\nabla\cdot\mathbf{v}\mathbf{I}\right), \quad (13)$$

$$\mathbf{q} = -\lambda'\nabla T - \sum_c \lambda_{\mathrm{v},c}\nabla T_c^{\mathrm{v}} - p\sum_c D_{Tc}\mathbf{d}_c + \sum_c \rho_c h_c \mathbf{V}_c, \quad (14)$$

$$\mathbf{q}_c^{\mathrm{vibr}} = -\lambda_{\mathrm{v},c}\nabla T_c^{\mathrm{v}}. \quad (15)$$

In the above equations, $\mathbf{d}_c$ is the diffusive driving force, D_{cd}, D_{Tc}, ζ, η, λ', λ_{vv} are the transport coefficients: binary diffusion, thermal diffusion, bulk and shear viscosity, thermal conductivity, and vibrational thermal conductivity coefficients, respectively. The relaxation pressure p_{rel} is connected with the cross-coupling effect between the stress tensor and the rates of nonequilibrium processes: chemical reactions, VV', and VT energy transitions; for more details see Refs. 24 and 25, where p_{rel} is expressed in terms of reaction affinities. Another cross effect is associated with the velocity divergence which appears in both normal stress and production rates. The expression for the heat flux in the multitemperature approximation (14) contains additional terms that take into account the transfer of energy associated with vibrational temperature gradients. Coefficients $\lambda_{\mathrm{v},c}$ describe the vibrational energy transfer between molecules of the same species. The thermal conductivity coefficient λ' in the MT approximation determines the energy transfer through the translational (λ'_{tr}) and the rotational (λ_{rot}) degrees of freedom: $\lambda' = \lambda'_{\mathrm{tr}} + \lambda_{\mathrm{rot}}$; prime indicates that λ'_{tr} is a partial thermal conductivity coefficient, which does not include thermal diffusion ratios. For subsequent theoretical formulations it is more convenient to use the effective transport coefficients $\lambda'_{c,\mathrm{tr}}$, $\lambda_{c,\mathrm{rot}}$, η_c, and ζ_c defined for mixture species as follows: $\lambda' = \sum_c x_c(\lambda'_{c,\mathrm{tr}} + \lambda_{c,\mathrm{rot}})$, $\eta = \sum_c x_c \eta_c$, $\zeta = \sum_c x_c \zeta_c$, x_c is the molar fraction of species c. Note that the species effective transport coefficients are introduced solely to clarify the physical sense of the slip boundary conditions derived later; for the evaluation of effective coefficients we use accurate transport algorithms rather than empirical data.

Rigorous kinetic-theory algorithms for calculating transport coefficients can be found in Ref. 2. They include calculation of collision integrals, bracket integrals, and solution of linear transport systems. Similar algorithms for the evaluation of chemical and energy production rates are developed in 24, 25, and 45; in the latter references, the production rates take into account cross-coupling effects between the production rates and normal stress as well as coupling of chemical reactions and vibrational energy transitions.

At this point, we have a closed system of transport equations for the MT set of fluid dynamic variables. The system of MT governing equations (6) consists of $L+4+L_{\mathrm{m}}$ equations, which are: the continuity equations for mixture components describing the change of species fractions due to chemical reactions and diffusion; the conservation of momentum taking into account viscous effects, including bulk viscosity; the total energy conservation equation; and, additionally for the MT model, the relaxation equations for the vibrational energy capturing its change due to inelastic VV' and VT collisions, and chemical reactions. The next step is to formulate an approach for deriving slip boundary conditions for this system of equations.

III. FORMULATION OF THE METHOD TO OBTAIN SLIP BOUNDARY CONDITIONS

Let us summarize some peculiarities of the method for deriving slip boundary conditions based on the kinetic boundary condition. The main idea lies in the ability to derive boundary conditions through a procedure similar to the derivation of transport equations from the Boltzmann equation. Such a method allows derivation of slip BCs for an arbitrary gas mixture flow model and, due to the known Chapman–Enskog procedure for the evaluation of mixture transport and chemical properties, provides a closed formulation of the boundary condition problem. Instead of the Boltzmann equation, this method uses a boundary condition for the distribution function, and the kinetic boundary condition[46] generalized for the chosen approximation of the mixture flow[43].

A. Modification of kinetic BC to include newly formed and desorbed species

First, we extend the kinetic BC to include processes that lead to an increase in particle number near the surface[28,44], which are chemical reactions resulting in gas species formation and a desorption from the solid surface. The kinetic boundary condition under these assumptions for the MT flow

description has the following form:

$$f^{+}_{cij}(\mathbf{r},\mathbf{u}_c,t)u_{cn}|_{u_{cn}>0} = \sum_{kl}\int\limits_{u'_{cn}<0} f^{-}_{ckl}(\mathbf{r},\mathbf{u}'_c,t)|u'_{cn}|T^{cij}_{ckl}\mathrm{d}\mathbf{u}'_c + \sum_{dkl}\gamma^{c}_{d}\int\limits_{u'_{dn}<0} f^{-}_{dkl}(\mathbf{r},\mathbf{u}'_d,t)|u'_{dn}|\tilde{T}^{cij}_{dkl}\mathrm{d}\mathbf{u}'_d + \mathtt{D}^{\mathrm{w}}_{c}\,\tilde{f}^{+,M}_{cij}(\mathbf{r},\mathbf{u}_c,t)u_{cn}|_{u_{cn}>0}, \tag{16}$$

where $f^{+}_{cij}(\mathbf{r},\mathbf{u}_c,t)$, $f^{-}_{cij}(\mathbf{r},\mathbf{u}_c,t)$ are the distribution functions of reflected and incident gas particles, $f^{+,M}_{cij}$ is the Maxwell–Boltzmann non-equilibrium distribution, depending generally on both T and T^{v}_{c} (i.e., the zeroth-order distribution function[2]). The scattering kernel[47,48], $T^{cij}_{ckl} = T^{cij}_{ckl}(\mathbf{u}_c,\mathbf{u}'_c)$, is the the probability density such that $T^{cij}_{ckl}\,\mathrm{d}\mathbf{u}_c$ gives the probability that a species ckl with the incident velocity $\mathbf{u}'_c$ will be scattered from the surface as a species cij with the velocity in the range $\mathbf{u}_c\,\mathrm{d}\mathbf{u}_c$. Here, due to the MT flow description, we assume rapid energy exchange with the surface in both rotational and vibrational modes, so the molecule may change its internal state during this rapid scattering process; note that in the StS formulation of the method, the rapid energy exchange was assumed for the rotational state only. The kernel $\tilde{T}^{cij}_{dkl} = \tilde{T}^{cij}_{dkl}(\mathbf{u}_c,\mathbf{u}'_d)$ is the reflection kernel for newly formed species, which has the same meaning as T^{cij}_{ckl}. The probability γ^{c}_{d} (where $d \neq c$) is the probability that a species d is involved in the formation process of a c species; $\mathtt{D}^{\mathrm{w}}_{c}$ is the species c desorption coefficient, defined as the ratio of the number flux of desorbed particles to the number flux of incident particles. From this point on, we assume that the reflection of newly formed species is diffuse ($\tilde{T}^{cij}_{dkl}(\mathbf{u}_c,\mathbf{u}'_d) = T^{cij}_{\mathrm{diff}}(\mathbf{u}_c)$):

$$T^{cij}_{\mathrm{diff}}(\mathbf{u}_c) = \frac{2}{\pi}\left(\frac{m_c}{2kT^{\mathrm{w}}}\right)^{2}\frac{s^{c}_{j}u_{cn}}{Z^{\mathrm{rot}}_{c}(T^{\mathrm{w}})Z^{\mathrm{vibr}}_{c}(T^{\mathrm{w}})} \times \exp\left(-\frac{m_c u^{2}_{c}}{2kT^{\mathrm{w}}} - \frac{\varepsilon^{c}_{j}}{kT^{\mathrm{w}}}\right)\exp\left(-\frac{\varepsilon^{c}_{i}}{kT^{\mathrm{w}}}\right). \tag{17}$$

Here, T^{w} is the wall temperature, s^{c}_{j} is the rotational statistical weight, and Z^{rot}_{c} is the rotational partition function. The desorption of species from the surface, as it can be seen from relation (16), is assumed to follow a Maxwell–Boltzmann distribution with the wall temperature. This is due by the fact, that both newly formed and desorbed species are assumed to be in thermal equilibrium with the surface. Justification for these assumptions and additional details on the inclusion of reaction processes can be found in Ref. 28.

An additional assumption made for the diffusive reflected kernel in the MT approximation is that the temperatures of all energy modes are set equal to the wall temperature. This is justified by the assumptions of full accommodation of chemical energy and thermal equilibrium state for the solid surface. As a result, the vibrational wall temperatures are also set equal to the wall temperature in the kernel. This diffuse scattering model will be further used in the derivation of the slip boundary conditions.

B. Incorporation of adsorption and processes that lead to particle loss

Another step in formulating the method for obtaining slip boundary conditions is to account for gas particle loss due to their participation in the formation of other gas particles or their adsorption on free surface sites. For this purpose, the normalization condition for the scattering kernel needs to be modified:

$$\sum_{ij}\int\limits_{u_{cn}>0} T^{cij}_{ckl}(\mathbf{u}_c,\mathbf{u}'_c)\mathrm{d}\mathbf{u}_c = 1 - \sum_{d}\gamma^{d}_{c} - \mathtt{S}^{\mathrm{w}}_{c}, \tag{18}$$

where $\mathtt{S}^{\mathrm{w}}_{c}$ is the sticking coefficient, which is the fraction of incident particles impinging on a surface that are really adsorbed. The relation above, when the right-hand side is equal to one, states that during the scattering process, a species with the incident velocity $\mathbf{u}'_c$ will, with probability equal to one, be scattered with the velocity $\mathbf{u}_c$ from the half-space (with a non-negative normal component) and occupy some rotational and vibrational levels from their respective sets. However, when surface chemical reactions occur, not all molecules and atoms can be scattered from the surface. Therefore, we must account for only the fraction of particles that can be scattered, which is given by $1 - \sum_d \gamma^{d}_{c} - \mathtt{S}^{\mathrm{w}}_{c}$. Incorporation of this fraction of lost particles into the scattering kernels can be arranged in two different ways.

1. *Flux based approach*

This approach was developed as a result of our initial formulation, which, with some simplifications, is equivalent to the Grad and Patterson–Shidlovskiy techniques[43], and is related to works where heterogeneous reactions are included in the boundary conditions, extending the Scott recombination model[49] (see details in Ref. 44). Within this formulation, the scattering kernel is split into two parts: one responsible for the scattering process, and another accounting for the fraction of particles that are lost. For the former, diffuse reflection is assumed, since newly formed or desorbed species are in thermal equilibrium with the surface. In the case of the Maxwell scattering model, the kernel under such an assumption has the form:

$$T^{cij}_{ckl,\mathrm{M}}(\mathbf{u}_c,\mathbf{u}'_c) = (1-\sigma_c)\delta_{lj}\delta_{ki}\delta(\mathbf{u}'_c - \mathbf{u}_c + 2u_{cn}\mathbf{n}) + \left(\sigma_c - \sum_{d}\gamma^{d}_{c} - \mathtt{S}^{\mathrm{w}}_{c}\right)T^{cij}_{\mathrm{diff}}(\mathbf{u}_c). \tag{19}$$

Here, σ_c is the accommodation coefficient for species c, representing the fraction of particles that are diffusely scattered from the solid surface.

Substituting an arbitrary kernel under this assumption into

the kinetic BC (16) allows rewriting it in the following form:

$$\begin{aligned} f^{+}_{cij}(\mathbf{r},\mathbf{u}_c,t)u_{cn}|_{u_{cn}>0} = &\sum_{kl}\int\limits_{u'_{cn}<0} f^{-}_{ckl}(\mathbf{r},\mathbf{u}'_c,t)|u'_{cn}|T^{cij}_{ckl}\mathrm{d}\mathbf{u}'_c \\ &+\sum_{dkl}\gamma^{c}_{d}\int\limits_{u'_{dn}<0} f^{-}_{dkl}(\mathbf{r},\mathbf{u}'_d,t)|u'_{dn}|\tilde{T}^{cij}_{dkl}\mathrm{d}\mathbf{u}'_d \\ &+\mathtt{D}^{\mathrm{w}}_{c}\tilde{f}^{+,M}_{cij}(\mathbf{r},\mathbf{u}_c,t)u_{cn}|_{u_{cn}>0} \\ &-\left(\sum_{d}\gamma^{d}_{c}+\mathtt{S}^{\mathrm{w}}_{c}\right)\sum_{kl}\int\limits_{u'_{cn}<0} f^{-}_{ckl}(\mathbf{r},\mathbf{u}'_c,t)|u'_{cn}|T^{cij}_{\mathrm{diff}}\mathrm{d}\mathbf{u}'_c, \end{aligned} \tag{20}$$

while the kernel T^{cij}_{ckl} now satisfies the common normalization condition:

$$\sum_{ij}\int\limits_{u_{cn}>0} T^{cij}_{ckl}(\mathbf{u}_c,\mathbf{u}'_c)\mathrm{d}\mathbf{u}_c = 1. \tag{21}$$

The obtained relation (20) indicates that the flux of particles lost in adsorption or chemical processes, is subtracted from the flux of particles reflected from the solid surface. Therefore, we call this model the Flux-based approach.

This procedure for accounting for lost particles was formulated under the assumption of small recombination probabilities. In Section V, we will demonstrate its limitations.

2. Kernel based approach

The flux-based approach was the only one considered in our previous works. However, it appears to be not entirely accurate, as it involves a scattering kernel for lost particles, which are not actually scattered. A more consistent way to incorporate species loss is through an additional multiplier applied to the scattering kernel — the fraction of particles that can indeed be scattered, given by $\left(1-\sum_d \gamma^d_c - \mathtt{S}^{\mathrm{w}}_c\right)$. For example, the Maxwell scattering kernel under the multitemperature flow description, when modified according to this new formulation, takes the following form:

$$\begin{aligned} T^{cij}_{ckl,\mathrm{M}}(\mathbf{u}_c,\mathbf{u}'_c) = &\left(1-\sum_{d}\gamma^{d}_{c}-\mathtt{S}^{\mathrm{w}}_{c}\right) \\ &\times\left((1-\sigma_c)\delta_{lj}\delta_{ki}\delta(\mathbf{u}'_c-\mathbf{u}_c+2u_{cn}\mathbf{n})+\sigma_c T^{cij}_{\mathrm{diff}}(\mathbf{u}_c)\right). \end{aligned} \tag{22}$$

The numerical assessment of this approach is carried out in Section V B.

At this stage, we have formulated a method for MT gas mixture flows based on the kinetic boundary condition. This was achieved by adapting to the MT flow description the main ideas of the previously developed state-to-state approach and by improving the treatment of gas particle loss. Our next objective is to obtain the boundary conditions for the set of fluid dynamic variables.

Note that in this work we focus on deriving boundary conditions for the specular-diffuse (Maxwell) scattering kernel (19), (22). In Ref. 28, we obtained the slip conditions for the Cercignani–Lampis (CL) model[48]. As for more physically detailed models, such as the Epstein model[50], they, as well as the CL model, are beyond the scope of this study, since they involve two or more parameters (e.g., energy accommodation coefficients), which are typically unknown for individual species of an arbitrary mixture. Therefore, we exclude these models from the present analysis and focus on the influence of contributions of different physical-chemical processes on the slip BCs in the case of the Maxwell scattering kernel.

IV. MULTITEMPERATURE SLIP BOUNDARY CONDITIONS

As already mentioned, the procedure for obtaining slip boundary conditions is similar to the derivation of transport equations from the Boltzmann equation within the framework of the Chapman–Enskog method. The only difference is that the integration is performed over the half-space $\{\mathbf{u}_c | u_{cn} > 0\}$. Multiplying the kinetic boundary condition (16) by the collision invariants of the rapid process, followed by integration and summation, allows one to obtain the boundary condition for the fluid dynamic variable corresponding to this microscopic invariant. Multiplying by the additional collision invariants (4) yields BCs for species concentrations; by (5), for vibrational temperatures; and by (3), yields velocity slip and temperature jump relations. Physically, before actually performing integration and summations, the resulting integral relation implies that the reflected flux of the corresponding macroparameter consists of three contributions: from scattered particles, from newly formed particles, and from desorbed ones. Besides that, the flux of scattered particles accounts for the fact that some species are lost during the gas-surface interaction.

While obtaining the slip BCs we make the following assumptions: 1) the expressions for the distribution functions of incident particles, $f^{-}_{cij}(\mathbf{r},\mathbf{u}'_c,t)$, and reflected particles, $f^{+}_{cij}(\mathbf{r},\mathbf{u}_c,t)$, are of the same form and order in the Knudsen layer, meaning that they depend on the same macroscopic quantities; 2) the distribution functions correspond to the first-order approximation of the Chapman–Enskog method[2] (i.e., we apply the viscous flow approximation); 3) we assume that the normal component of the macroscopic velocity is zero, $\mathbf{v}\cdot\mathbf{n}|_{\mathrm{w}} = 0$ (this equation can be derived explicitly when surface reactions are neglected; otherwise, it is introduced as an additional assumption); 4) finally, we neglect the relaxation pressure since its contribution to the normal stress in MT flows is about 1-2% of p, see Ref. 24.

For brevity, the detailed derivation of the multi-temperature boundary conditions is not presented here. A concise outline of the derivation and the key simplification steps are provided in the Supplementary Material.

A. Mass fluxes near surface

We first derive the relations for the mass fluxes near the wall. As in the state-to-state approximation, the expressions for the species mass fluxes do not depend on the scattering kernel T_{ckl}^{cij} itself, but rather on its normalization condition (18) and the type of the reflection kernel $\tilde{T}_{dkl}^{cij}$. Performing the above mentioned procedure, we obtain:

$$\begin{aligned}\sum_{ij}\int\limits_{u_{cn}>0} u_{cn} f_{cij}^{+}\mathrm{d}\mathbf{u}_c = \\ -\left(1-\sum_d \gamma_c^d - \mathrm{S}_c^{\mathrm{w}}\right)\sum_{kl}\int\limits_{u'_{cn}<0} f_{ckl}^{-}u'_{cn}\mathrm{d}\mathbf{u}'_c \\ -\sum_{dkl}\gamma_d^c\int\limits_{u'_{dn}<0} f_{dkl}^{-}u'_{dn}\mathrm{d}\mathbf{u}'_d + \mathrm{D}_c^{\mathrm{w}}\sum_{ij}\int\limits_{u_{cn}>0} u_{cn}\tilde{f}_{cij}^{+,M}\mathrm{d}\mathbf{u}_c.\end{aligned} \tag{23}$$

Here $f_{cij}^{+} = f_{cij}^{+}(\mathbf{r},\mathbf{u}_c,t)$, $f_{ckl}^{-} = f_{ckl}^{-}(\mathbf{r},\mathbf{u}'_c,t)$. Substituting the the first-order approximation of the distribution function[2], we obtain the following expressions for the mass fluxes of gaseous species near the surface:

$$\begin{aligned}\left(2-\sum_d \gamma_c^d - \mathrm{S}_c\right)\mathbf{J}_c\cdot\mathbf{n} = -\frac{\left(\sum_d \gamma_c^d + \mathrm{S}_c\right)\rho_c}{n\sqrt{2\pi m_c kT}}\left(p+P_{nn,c}\right) \\ +\sqrt{\frac{2kT^{\mathrm{w}}}{\pi m_c}}\rho_c\mathrm{D}_c - \sum_d \frac{\gamma_d^c m_c}{m_d}\mathbf{J}_d\cdot\mathbf{n} + \frac{1}{\sqrt{2\pi kT}}\sum_d \frac{\gamma_d^c m_c \rho_d}{n\sqrt{m_d^3}}\left(p+P_{nn,d}\right),\end{aligned} \tag{24}$$

The velocity slip includes contributions from viscous stress, tangential translational energy flux, and species mass fluxes. These terms are highly affected by the accommodation coefficients.

The temperature jump, in the case of the scattering model given by (19), can be written as follows:

$$\frac{T}{T^{\mathrm{w}}} = \frac{\sum_c \frac{2-\sigma_c}{m_c}\left(1+\frac{m_c v^2}{4kT^{\mathrm{w}}}+\frac{m_c E_{\mathrm{rot},c}(T^{\mathrm{w}})}{2kT^{\mathrm{w}}}\right)\mathbf{J}_c\cdot\mathbf{n} + \sqrt{\frac{2}{\pi kT}}\sum_c \sigma_c \frac{n_c}{2n\sqrt{m_c}}\left(1+\frac{m_c v^2}{4kT^{\mathrm{w}}}+\frac{m_c E_{\mathrm{rot},c}(T^{\mathrm{w}})}{2kT^{\mathrm{w}}}\right)\left(p+P_{nn,c}\right)}{\sum_c \frac{2-\sigma_c}{m_c}\left(\frac{5}{4}+\frac{m_c E_{\mathrm{rot},c}(T)}{2kT}\right)\mathbf{J}_c\cdot\mathbf{n} - \sum_c (2-\sigma_c)\frac{n_c}{2kn}\lambda'_c\frac{\partial \ln T}{\partial n} + \sqrt{\frac{2}{\pi kT}}\left(Y_1+Y_2+Y_3\right)}, \tag{26a}$$

$$Y_1 = \sum_c \sigma_c \frac{3n_c}{2n\sqrt{m_c}}\left(2/3p - \eta_c S_{nn} - \zeta_c \nabla\cdot\mathbf{v}\right); \tag{26b}$$

$$Y_2 = T\sum_c \sigma_c \frac{n_c}{2n}\sqrt{m_c}\,\frac{c_{\mathrm{rot},c}}{k} f_{c,01}\nabla\cdot\mathbf{v}; \tag{26c}$$

$$Y_3 = \sum_c \sigma_c \frac{n_c}{4n\sqrt{m_c}}\frac{m_c E_{\mathrm{rot},c}(T)}{kT}\left(p+P_{nn,c}\right). \tag{26d}$$

Here, $f_{c,01}$ is the expansion coefficient that appears in the first-order correction to the distribution function when

where $c = 1,\ldots,L$, $P_{nn,c} = p+\tau_{nn,c} = p - 2\eta_c S_{nn} - \zeta_c \nabla\cdot\mathbf{v}$, n is the total number density of gas mixture, $n = \rho R/(kM_{\mathrm{mix}})$ (n_c is the c species number density). This expression is similar to the one obtained in the state-to-state approximation[28]. Moreover, the obtained expressions have a form similar to the relations rigorously derived in Ref. 51, where physisorbed and chemisorbed species are explicitly taken into account. The mass flux of species c consists of four parts: 1) the backward flux of particles of the same species, accounting for their loss due to participation of c-species in the formation of other species or adsorption; 2) the flux of desorbed c-species; 3) the backward mass fluxes of species that are involved in the formation of c species; 4) the flux of species that participate in the formation of c-species. The third contribution requires some clarification, while the others are straightforward. This flux is included to account for the fact that d species are both lost and can also be formed due to surface reactions. The system of equations including the mass fluxes (24), captures all contributions of surface processes to species fluxes simultaneously. In addition, the system is affected by slip effects in the gas.

B. Velocity slip and temperature jump

The velocity slip depends on the chosen type of scattering kernel. For specular-diffusive scattering in the form of (19), we obtain the following relation for the velocity component v_l, which is also similar to the expression in the STS approximation:

$$v_l = \frac{\sqrt{\frac{2\pi}{kT}}\sum_c \frac{(2-\sigma_c)n_c}{n}2\eta_c S_{ln} + \frac{1}{5kn}\sum_c \sigma_c n_c\sqrt{m_c}\lambda'_{\mathrm{tr},c}\frac{\partial \ln T}{\partial \tau_l} - \sum_c \frac{\sigma_c}{\sqrt{m_c}}\mathbf{J}_c\cdot\boldsymbol{\tau}_l}{\sqrt{\frac{2\pi}{kT}}\sum_c \frac{\sigma_c}{2}\mathbf{J}_c\cdot\mathbf{n} + \sum_c \frac{\sigma_c\sqrt{m_c}n_c}{2nkT}\left(p+P_{nn,c}\right)}. \tag{25}$$

it is expanded into the series of Sonine and Waldmann–Trübenbacher polynomials[2]. This coefficient is not directly related to any effective transport coefficient and is therefore kept in this form; in the MT approach, it represents the influence of rotational relaxation and can be implicitly connected to the bulk viscosity coefficient. The rotational specific heat for species c is defined as $c_{\mathrm{rot},c} = \partial E_{\mathrm{rot},c}(T)/\partial T$. In this work, since we consider the rigid rotator model for the rotational motion, the rotational specific heat and the rotational energy are given by (10): $c_{\mathrm{rot},c} = k/m_c$ and $E_{\mathrm{rot},c}(T) = kT/m_c$. Applying these relations, the temperature jump takes a simplified form:

$$\frac{T}{T^{\mathrm{w}}} = \frac{\sum\limits_c \frac{2-\sigma_c}{m_c}\left(\frac{3}{2}+\frac{m_c v^2}{4kT^{\mathrm{w}}}\right)\mathbf{J}_c\cdot\mathbf{n} + \sqrt{\frac{2}{\pi kT}}\sum\limits_c \sigma_c \frac{n_c}{2n\sqrt{m_c}}\left(\frac{3}{2}+\frac{m_c v^2}{4kT^{\mathrm{w}}}\right)(p+P_{nn,c})}{\sum\limits_c \frac{2-\sigma_c}{m_c}\frac{7}{4}\mathbf{J}_c\cdot\mathbf{n} - \sum\limits_c (2-\sigma_c)\frac{n_c}{2kn}\lambda_c'\frac{\partial \ln T}{\partial n} + \sqrt{\frac{2}{\pi kT}}\left(Y_1+Y_2+\sum\limits_c \sigma_c \frac{n_c}{4n\sqrt{m_c}}(p+P_{nn,c})\right)}. \tag{27}$$

Despite the similarities between the temperature jump (TJ) obtained in the multitemperature approximation (26) and the one derived within the framework of the STS approach[43], the new relation additionally accounts for the relaxation of rotational energy resulting from the gas interaction with the solid surface; this result is obtained for the first time in the present work. Note that the STS temperature jump[43] can also be updated by taking into account rotational energy transitions. Later, we will examine its impact in Sec. V D.

As for the derivation of the velocity slip and temperature jump in the case of the specular-diffusive scattering kernel (22) correctly modified to account for the particle loss, the resulting relations retain exactly the same general form. The only difference is that, instead of the original accommodation coefficients for species c, σ_c, we now have modified coefficients, $\tilde{\sigma}_c$, defined as:

$$\tilde{\sigma}_c = \sigma_c + (1-\sigma_c)\left(\mathrm{S}_c^{\mathrm{w}} + \sum_d \gamma_c^d\right). \tag{28}$$

These modified coefficients imply that, when species participate in the formation of others, their scattered flux exhibits a higher accommodation coefficient, i.e. more particles are scattered diffusely. This corresponds to a higher degree of rotational-translational energy accommodation. However, it should be noted that this effect occurs only when the solid surface is in thermal equilibrium.

C. Vibrational temperature jump

The remaining boundary conditions for vibrational temperatures, or vibrational temperature jumps, can be written in terms of the vibrational energy flux. These relations also depend on the chosen type of scattering model. In the case of the model (19), applying the procedure to the kinetic boundary condition (16) with vibrational energy as the collision invariant (5) results in the following relations:

$$\begin{aligned}\mathbf{q}_{\mathrm{vibr},c}\cdot\mathbf{n} = &-\left(E_{\mathrm{vibr,c}}(T_c^{\mathrm{v}}) - E_{\mathrm{vibr,c}}(T^{\mathrm{w}})\right)\mathbf{J}_c\cdot\mathbf{n} \\ &- \frac{\sigma_c}{2-\sigma_c}\left(E_{\mathrm{vibr,c}}(T_c^{\mathrm{v}}) - E_{\mathrm{vibr,c}}(T^{\mathrm{w}})\right) \\ &\times\sqrt{\frac{m_c}{2\pi kT}}(p+P_{nn})\frac{n_c}{n}.\end{aligned} \tag{29}$$

The above boundary condition implies that the vibrational energy flux of species c changes due to two contributions. The first term is the impact of the mass flux of species c, which appears only if surface chemical processes occur. This term accounts not only for the vibrational energy change due to the formation of new molecules but also due to their loss. The second contribution is directly associated with the Maxwell scattering model and reflects how the vibrational energy flux depends on the fraction of diffusely reflected particles. Besides that, this second part also depends on the fraction of c molecules.

Again, in the case of the Kernel approach for particle loss (22), the accommodation coefficients are replaced by the modified expressions (28).

It is important to note that these theoretical boundary conditions for vibrational temperatures (29) are obtained for the first time. It is also worth emphasizing that no phenomenological assumptions were introduced during their derivation. Despite the simplified model of vibrational energy change during particle scattering, the relations still yield interesting results and capture the effect of vibrational temperature variation under the Maxwell scattering model. More physically accurate models can be derived in a similar manner; however, they are not considered in this work, as their implementation would require either the probabilities of species vibrational state–surface transitions or more advanced models based on reaction rates. To our knowledge, such models do not yet exist, but they could be developed in the future using Molecular Dynamics simulations and easily incorporated into the proposed framework.

Let us now compare the derived expressions for the vibrational temperature jump (29) with other models existing in the literature. In most of the studies[32,36–38,40,42], the vibrational TJ has the following form (in most cases scattering of

particles is specular-diffusive, however, in some cases it is not specified and relations are obtained by introducing additional accommodation coefficient for vibrational energy):

$$T_{\rm v} - T_{\rm v}^{\rm w} = \zeta_v F(\text{gas properties}, \sigma_{\rm v})\, \mathbf{q}_{\rm vibr} \cdot \mathbf{n}, \qquad (30)$$

or, alternatively, in the form where the vibrational temperatures in the LHS ($T_{\rm v}$ is the vibrational temperature common for all the components (two-temperature model), $T_{\rm v}^{\rm w}$ is the wall vibrational temperature) are replaced by the vibrational energies:

$$E_{\rm vibr}(T_{\rm v}) - E_{\rm vibr}(T_{\rm v}^{\rm w}) = \zeta_v F \frac{\partial E_{\rm vibr}(T_{\rm v})}{\partial n}. \qquad (31)$$

Here, $\sigma_{\rm v}$ is the vibrational energy accommodation coefficient, $F(\cdot)$ is the scaling function depending on relaxation parameters and transport properties in the mixture. Larini and Brun[36] were among the first to obtain the vibrational TJ. The relation was derived for the Enskog–Morse distribution and the BGK form of the Boltzmann equation; the solution was obtained by numerically solving some parts of the conservation laws and employing the solutions into accommodation coefficient definitions[36]:

$$T_{\rm v} - T^{\rm w} = \frac{2-\sigma_{\rm v}}{2\sigma_{\rm v}} \frac{1}{\Theta} \sqrt{\frac{2\pi k T^{\rm w}}{m}} \frac{\partial T_{\rm v}}{\partial n}, \qquad (32)$$

where Θ is the collision frequency including elastic and pure rotational processes[38]. The above vibrational temperature jump cannot be obtained directly from Eq. (29). However, a similar form can be derived if we neglect: (i) the impact of heterogeneous processes on the vibrational temperature; (ii) viscous effects; and (iii) the influence of the gas temperature near the wall, thus accounting only for the wall temperature. Furthermore, Eq. (32) is derived under assumption that the vibrational energy has the simplified form $E_{\rm vibr,c}(T^{\rm v}) = kT^{\rm v}/m$, which does not take into account varying vibrational specific heats. In our relation, we use the correct definition of the vibrational energy and additionally account for the molecular concentrations. However, in our vibrational TJ we do not include a separate accommodation coefficient for the vibrational energy. This is indeed a limitation; however, as mentioned above, it can be overcome by introducing the previously mentioned probabilities for different types of particle scattering.

Another form of the vibrational TJ was introduced in the works of Gökçen, e.g. see Ref. 37:

$$E_{\rm vibr}(T_{\rm v}) - E_{\rm vibr}(T_{\rm v}^{\rm w}) = \frac{2-\sigma_{\rm v}}{\sigma_{\rm v}} \cdot \text{MFP} \cdot \frac{\partial E_{\rm vibr}(T_{\rm v})}{\partial n}, \qquad (33)$$

where MFP is the mean free path for the transport of momentum[32]. The relation was later modified to the following form in Ref. 42:

$$T_{\rm v} - T^{\rm w} = \frac{2-\sigma}{\sigma} \cdot Z_v \cdot \text{MFP} \cdot \frac{\partial T_{\rm v}}{\partial n}. \qquad (34)$$

A common accommodation coefficient is applied for translational and rotational temperature jumps; an additional factor, Z_v, is used to account for the vibrational energy accommodation.

The above relations also cannot be directly obtained from our vibrational TJ expression. However, similar forms can be derived with the same simplifications (i)–(iii). Still, these relations do not account for surface reactions and slip effects as well as for the mutual influence of translational-rotational and vibrational temperatures on the gas parameters near the wall.

Another two-temperature model was introduced by Kosuge et al.[40], where, instead of a vibrational TJ, a boundary condition was formulated for the internal temperature. The relation is written in general form (30) and additionally accounts for the density of molecular components in the mixture, but it is obtained under the assumption of full vibrational energy accommodation. Still, the relation does not account for mutual slip effects or heterogeneous processes that influence the vibrational temperature, as is done in our model.

A model introducing the vibrational temperature for each molecular component of the gas mixture was presented in a work of Kiruytin and Tirskiy[39]. The Maxwell–Loyalka method was applied to obtain a set of slip BCs under the specular-diffusive scattering model. Their formulation includes separate accommodation coefficients for translational-rotational and vibrational energies. The BC for the vibrational temperature is the most similar to that derived in the present study; however, the model 39 also does not include slip effects or heterogeneous reactions. The novelty of the model is that it includes two accommodation coefficients, which is not found in any other works. In our study, we assume full accommodation during diffusive scattering, though this limitation can be overcome.

Additionally, several numerical and experimental works[5,32,38,42,52–54] show that in some cases, near a plane wall or in hypersonic double-cone simulations, the vibrational temperature remains frozen in certain regions of the boundary layer. Consequently, an adiabatic condition for the vibrational temperature has been proposed ($\sigma_{\rm v} \approx 0$, $\mathbf{q}_{\rm vibr} \cdot \mathbf{n} = 0$)[5,38,42]. Such a model can be considered as one of the particular cases of our model.

D. Particular case of boundary conditions

Let us rewrite the boundary conditions in the case when the velocity slip is neglected and, from all the described surface processes, only heterogeneous recombination is considered. Such a simplified model of gas–solid surface interaction is applied to investigate the effects from particle loss model, rotational energy relaxation due to gas–surface interactions and the impact of the model on the heat flux. In order to neglect the mutual influence of surface reactions and focus only on model effects, we consider a single heterogeneous process. This can be done since our model does not account for step-by-step surface reactions[55], implying that the recombination probability γ_c^d already incorporates the full heterogeneous recombination reaction mechanism (Eley–Rideal or Langmuir–Hinshelwood). As for the velocity slip, its effects can be ne-

glected, for example, near the stagnation line, where one of the peak heating zones of the surface occurs.

The species concentration boundary conditions (24) under these simplifications take the following form:

$$\mathbf{J}_{\mathrm{A}}\cdot\mathbf{n} = -\sqrt{\frac{2kT}{\pi m_{\mathrm{A}}}}\,\frac{\sum_{\mathrm{M}}\gamma_{\mathrm{A}}^{\mathrm{rec,M}}}{2-\sum_{\mathrm{M}}\gamma_{\mathrm{A}}^{\mathrm{rec,M}}}\,\rho_{\mathrm{A}}; \tag{35}$$

$$\begin{aligned}\mathbf{J}_{\mathrm{AB}}\cdot\mathbf{n} = &-\frac{1}{2}\sum_{s=\mathrm{A,B}}\frac{\gamma_s^{\mathrm{rec,AB}}}{2}\,\frac{m_{\mathrm{AB}}}{m_s}\,\mathbf{J}_s\cdot\mathbf{n}\\ &+\frac{1}{2}\sqrt{\frac{2kT}{\pi}}\sum_{s=\mathrm{A,B}}\frac{\gamma_s^{\mathrm{rec,AB}}}{2}\,\frac{m_{\mathrm{AB}}}{m_s}\,\frac{\rho_s}{\sqrt{m_s}}.\end{aligned} \tag{36}$$

Here, A is an atom; M and AB are molecules (with AB composed of A and B atoms); $\gamma_s^{\mathrm{rec,AB}}$ is the probability that molecule AB is formed with the participation of atom s. The additional division of this probability by 2 in the molecular mass flux expressions (36) is due to the definition of γ: since it refers to the entire reaction event, the contribution is split between the two participating atoms.

The general mass flux expression (24) is split here into two separate relations for the mass fluxes of atoms and molecules for convenience. As can be seen from the provided relations, in the case when only recombination is considered and the mixture consists of atoms and diatomic molecules, the mass fluxes can be calculated explicitly, without solving a system of linear equations, as is required in the case of general expression for the mass flux near the surface.

The temperature jump (27), when the velocity slip is neglected, can be rewritten as follows:

$$\frac{T}{T^{\mathrm{w}}} = \frac{\sum_c \frac{3(2-\sigma_c)}{2m_c}\,\mathbf{J}_c\cdot\mathbf{n} + \sqrt{\frac{2kT}{\pi}}\sum_c \sigma_c\,\frac{3n_c}{2\sqrt{m_c}}}{\sum_c \frac{7(2-\sigma_c)}{4m_c}\,\mathbf{J}_c\cdot\mathbf{n} - \sum_c (2-\sigma_c)\,\frac{n_c}{2kn}\lambda_c'\frac{\partial \ln T}{\partial n} + \sqrt{\frac{2kT}{\pi}}\sum_c \sigma_c\,\frac{3n_c}{3\sqrt{m_c}}}. \tag{37}$$

The vibrational temperature jumps (29) in this particular case take the following form:

$$\begin{aligned}\mathbf{q}_{\mathrm{vibr},c}\cdot\mathbf{n} = &-\left(E_{\mathrm{vibr,c}}(T_c^{\mathrm{v}}) - E_{\mathrm{vibr,c}}(T^{\mathrm{w}})\right)\mathbf{J}_c\cdot\mathbf{n}\\ &-\frac{\sigma_c}{2-\sigma_c}\left(E_{\mathrm{vibr,c}}(T_c^{\mathrm{v}}) - E_{\mathrm{vibr,c}}(T^{\mathrm{w}})\right)\sqrt{\frac{2kT}{\pi m_c}}\,\rho_c.\end{aligned} \tag{38}$$

From here on, we will study the system of Eqs. (35)–(38). As can be seen, the system is nonlinear not only due to the presence of explicit nonlinear terms, but also because of the transport coefficients. The details of the numerical implementation, as well as the results of calculations, are presented in the following section.

It should be emphasized that the proposed description of non-equilibrium gas–surface interaction is fully closed from the fluid dynamic point of view. However, in the sense of surface chemistry, the determination of all surface chemical processes is still required. In particular, the sticking, desorption coefficients and heterogeneous reaction probabilities depend not only on the properties of the gas species and the solid wall, but also on the parameters of the impinging mixture flow. Numerous studies have addressed the evaluation of surface reaction probabilities or rate constants. There are phenomenological models that rely on recombination probabilities[56–59] obtained by fitting experimental data to derive their temperature dependence. The coefficients also can be obtained through rigorous modeling and subsequently fitted to a regression function, e.g. see work of Molchanova et al. 60, where coefficients for both Eley–Rideal and Langmuir–Hinshelwood recombination mechanisms are determined based on incident flow characteristics within DSMC modeling. Other works analyze heterogeneous recombination mechanisms through reaction rates. In Refs. 61–64, elementary-stage rate constants for surface reactions are considered, and, based on phenomenological assumptions about changes in species concentrations or heat fluxes with experimental recombination probability data, models for reaction rates are developed. More detailed investigations are presented in 65 and 66, where specific recombination mechanisms and their dependence on surface conditions are analyzed. However, the lack of direct data on surface concentrations and gas-phase species near the surface introduces significant uncertainties. To address these limitations, recent studies employ quasi-classical trajectory calculations or molecular dynamic simulations, see e.g. 55, 67–69, to describe the interaction of gas-phase species with the atomic structure of heat-shielding surfaces at the microscopic level.

Modeling surface chemistry is beyond the scope of our study; we rather carry out a parametric study using the recombination probability as a varying parameter.

V. RESULTS AND DISCUSSION

In this section, we discuss the impact of different models and processes on the slip boundary conditions (35)–(38). The calculations are performed for four mixtures containing air components: N_2/O_2/NO/N/O, O_2/O, NO/N/O, and N_2/N. As is mentioned above, among all surface reactions, only heterogeneous recombination is considered. We carry out a parametric study varying the model, the recombination probability, the accommodation coefficient, the mixture composition, the wall temperature, and the Knudsen number. Note that we do not consider any specific flow but evaluate the effect of the model directly on the temperature jumps, species molar fractions, and heat flux. Application of the developed BCs for nonequilibrium flow simulations will be done in the future work.

Since we do not consider a particular gas mixture flow problem, the recombination probabilities are not computed from the gas-phase data but are instead set to constant values; it is convenient for the parametric study. Moreover, we use constant values for the gas-phase macroscopic quantities and the wall temperature.

In our simulations, we fix the gas-phase temperature at $T = 1600$ K and the pressure at $p = 1000$ Pa; these conditions correspond to the Knudsen number near the wall of

$O(10^{-4})$ to $O(10^{-5})$ (values vary for different mixtures). The gas-phase compositions are set to 40% molecules and 60% atoms. In most cases, these concentrations are distributed equally among the molecular and atomic components, since the effects of individual species are less significant than the overall ratio of molecules to atoms. The accommodation coefficients in the Maxwell kernel are set to 0.55; more details on their impact on the parameters can be found in Ref. 70. The cell size in this work is equal to two mean free paths. The wall temperature T^{w} is varied and set to either 500 or 1000 K (cold wall) and 3000 K (hot wall).

In the parametric study, we compare dimensionless relative change of gas flow parameters for different models rather than the fluid dynamic variables themselves. Thus, we introduce relative variations of molar fractions, temperature, and vibrational temperatures

$$\Delta x_c = \frac{x_c^{\mathrm{BC}} - x_c^{\mathrm{gas}}}{x_c^{\mathrm{gas}}} \cdot 100\%, \quad \Delta T = \frac{T^{\mathrm{BC}} - T^{\mathrm{w}}}{T^{\mathrm{gas}}} \cdot 100\%,$$
$$\Delta T_c^{\mathrm{v}} = \frac{T_{\mathrm{c}}^{\mathrm{v,BC}} - T_c^{\mathrm{v,gas}}}{T_c^{\mathrm{v,gas}}} \cdot 100\%. \tag{39}$$

Here, the superscript 'BC' corresponds to the macroparameter calculated using the derived expressions for boundary conditions, 'gas' to the fixed gas-phase value of this parameter. Note that the relative temperature variation ΔT is calculated with respect to both the gas-phase and wall temperatures to allow a consistent comparison and better understanding of how the difference between them affects the results.

A. Implementation of slip BCs in codes

The general system of boundary conditions is a nonlinear system of differential equations. When discretized using a finite-difference scheme, it becomes a nonlinear algebraic system. Here, we use a forward difference with a step size of several mean free path lengths. Commonly, in continuum approaches, such a value is used for the mesh scale near the surfaces.

The system of Eqs. (35)–(38), where the velocity slip is neglected, can be decoupled to two subsystems, that are solved independently and sequentially: 1) the system of mass fluxes (35)–(36) and translational-rotational temperature jump (37); 2) the system of BCs for vibrational temperatures (38). The possibility of decoupling of these two subsystems directly follows from the boundary condition relations. Such decoupling reduces computation time by nearly half, and the difference between the obtained solutions is typically less than 1%. However, mass fluxes and the temperature jump in Eqs. (35)–(36) cannot be separated, since diffusion coefficients strongly depend on temperature, and the temperature jump is affected by species fractions and mass fluxes.

To ensure that the sum of molar or mass fractions is unity, the system of mass flux equations is solved together with the temperature jump relation L times (where L is the number of mixture components), each time replacing one mass flux equation with the normalization condition for fractions. This procedure allows solving the system for arbitrary recombination probabilities. The error introduced by this method depends on the probability value and, in the case of a fully catalytic wall, is less then 1%. For smaller probabilities, the error is negligible.

Non-linear systems can be solved numerically using standard algorithms available in most libraries, such as MINPACK and its wrappers. However, a solver for calculating transport coefficients is required. We developed an in-house solver capable of calculating these coefficients within both one-temperature and multitemperature approaches for arbitrary gas mixtures. The solution time for the described scheme depends on the initial conditions and mixture type but is typically about 0.1 sec in a single stream on a processor with a base frequency of 2.9 GHz. This value can be further reduced if necessary.

Once the solver for the BCs system is implemented, the subsequent integration of slip BCs into codes can be performed using standard schemes for implementing gas–solid wall boundary conditions. For some basic methods, examples for finite-difference schemes can be found in Ref. 28; for finite-volume, in Ref. 71.

B. Temperature jumps and molar fractions near the wall

First we briefly discuss the limits of applicability of the scattering kernel introduced previously for the description of the particle loss (see Eq. (19)) with respect to a more accurate formulation given by Eq. (22). For the sake of brevity, we further refer to the approach based on Eq. (19) as 'Flux model', and that based on Eq. (22) as 'Kernel model'.

Under conditions of our parametric study, the species molar fractions and vibrational temperature jumps are weakly affected by the choice of the particle loss model; the effect slightly increases with the recombination probability but does not exceed 5% in the entire range of parameters. On the contrary, the influence of the model on the temperature jump is significant, which can be seen in Figs. 1 and 2, where the relative temperature jumps ΔT are plotted as functions of the maximum atom loss probability and accommodation coefficient. In Fig1. 1, we compare the TJs calculated using the Flux and Kernel approaches applied to different mixtures for the cases of cold and hot wall. The results are shown for $\gamma > 0.2$ since for lower γ values, the effect is negligible. One can see that in all cases ΔT strongly varies with γ but weakly depends on the mixture composition.

For the cold wall, the Flux and Kernel models yield opposite trends of ΔT for $\gamma > 0.4$. For the Flux model, the increase in temperature is explained by the fact that species participating in recombination are excluded from the reflected flux, so the part of the flux that would have reflected with the wall temperature is lost. In the Kernel model, the temperature decreases with γ because a significant number of species are not scattered but transformed into others and then reflect at the wall temperature. As a result, the temperature jump becomes sensitive to the number of newly formed species, reducing at high γ. For the hot surface, the temperature jumps obtained

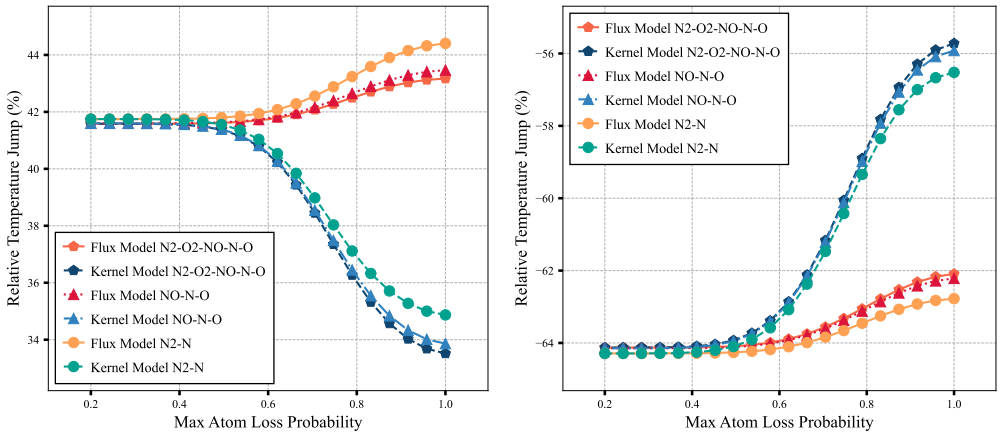

FIG. 1. Relative temperature variation ΔT as a function of maximum recombination probability; comparison of approaches to accounting for particle loss. Wall temperature: $T^{\mathrm{w}} = 500$ K (left); $T^{\mathrm{w}} = 3000$ K (right).

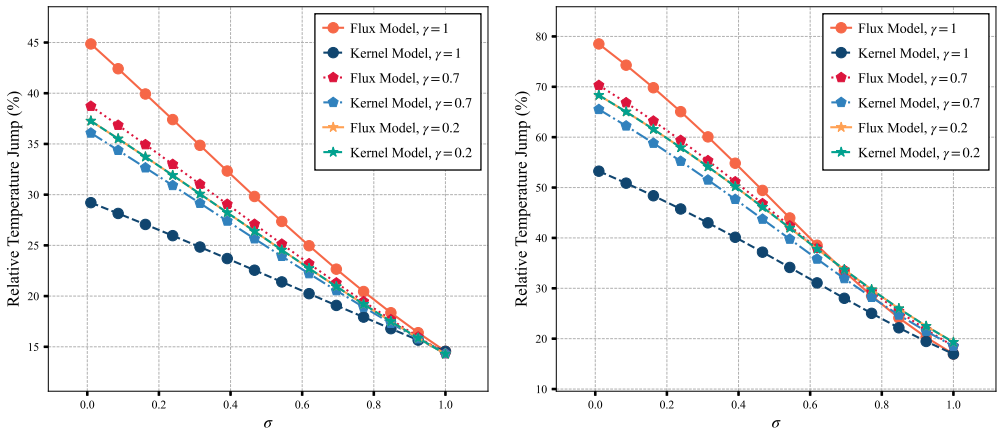

FIG. 2. Relative temperature variation ΔT as a function of accommodation coefficient; NO/N/O mixture; comparison of approaches to accounting for particle loss. Wall temperature: $T^{\mathrm{w}} = 1000$ K (left); $T^{\mathrm{w}} = 500$ K (right).

using the two approaches show a similar qualitative trend with the recombination probability: their absolute values decrease with γ because newly formed species are reflected into the gas with $T^{\mathrm{w}} > T$. In the Flux model, the TJs are lower since particles that should be reflected with the wall temperature are simply lost, leading to the underestimation of ΔT.

The above observations demonstrate better physical consistency of the Kernel model. Still, the Flux model can be used under conditions of moderate wall catalyticity and dominating diffusive reflection. It is seen from Fig. 2, where ΔT is plotted as a function of accommodation coefficient σ at fixed values of γ. It is interesting that the temperature jump exhibits almost linear dependence on σ. One can see that for $\gamma < 0.7$ and $\sigma > 0.5$ both models yield close ΔT values. Thus, for aerospace applications, where the wall catalyticity is supposed to be low and specular reflection is unlikely, both the Flux and the Kernel models can potentially be used. However, we recommend employing a more accurate Kernel model since in real flow simulations, minor deviations in the BCs may affect the fluid dynamic variables in a more pronounced way than in

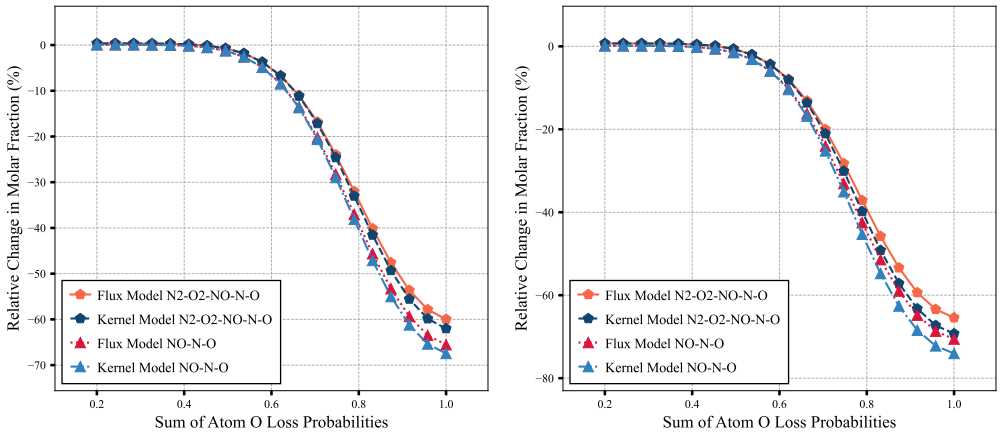

FIG. 3. Relative changes in the molar fractions of oxygen atoms Δx_O in various mixtures; comparison of approaches to accounting for particle loss. Wall temperature: $T^w = 1000$ K (left); $T^w = 500$ K (right).

the present parametric study.

Figure 3 shows the relative change in the fractions of oxygen atoms Δx_O in various mixtures, depending on the recombination probability γ that an O atom participates in recombination reactions to form other species. The dependence of molar fractions near the wall on the atom O loss probability is chosen to enable comparison between different mixtures. As is mentioned above, the largest effect of the particle loss model (about 5%) is observed at high γ; the discrepancy is mainly due to the Flux/Kernel model impact on the temperature jumps. Variations in the molar fractions in different mixtures arise from differences in species concentrations and how each mixture responds to the catalytic properties of the surface.

Besides that, in Fig. 3, we observe a strong impact of recombination probabilities on species concentrations starting from $\gamma > 0.4$. The molar fraction variations reach up to 70-75% for the fully catalytic wall case. It is worth mentioning that the obtained values are specific to the considered set of gas-phase macroscopic quantities. However, the overall extreme impact of high recombination probabilities on gas-phase fluid dynamic variables will remain. The wall temperature value also affects the mass fractions: for smaller T^w values, and thus smaller temperature values near the wall, the catalytic effects are more pronounced. This is due to the well-known fact that the higher the gas temperature near the surface, the lower the catalytic efficiency due to the increased gas species velocities, and, consequently, reduced surface adsorption ability.

In the next sections, we use only the Kernel approach for the particle loss description and focus on the cold wall cases since they are more relevant for high-speed aerodynamics.

C. Vibrational temperatures variations due to gas–surface interactions

Let us now evaluate the vibrational temperature jumps. Here we consider the five-component air mixture. As before, the same gas-phase parameters and accommodation coefficients are used. The gas-phase vibrational temperatures are set to either 700 K or 2000 K (the same temperature for all species), and the wall temperatures, are set to 500 K and 1000 K. These variations in vibrational temperatures allow us to capture different degrees of non-equilibrium in the system and to examine how the vibrational temperature is affected by gas species–wall interactions. The results for the Kernel model are presented in Figs. 4–5 in terms of relative vibrational temperature variations, ΔT_c^v.

The variations in species vibrational temperatures are primarily related to differences in their concentrations and formation rates. Figure 4 presents the results for an initial vibrational temperature higher than the gas-phase temperature. In this case, vibrational deactivation occurs: the results for low γ reflect the effects of molecular scattering at the surface, while cases with high γ also include the effects of heterogeneous recombination. As can be seen, the latter has a considerable impact on vibrational temperature variations. The greater the gap between the gas-phase temperature and the wall temperature, the more significant the vibrational relaxation toward equilibrium (i.e., the vibrational temperature predicted by the slip BC approaches the wall temperature).

Figure 5 presents the results for the case when the initial vibrational temperatures are lower than the gas-phase temperature. The results strongly depend on the species composition. When the wall temperature is higher than the vibrational temperature, some species tend toward equilibrium more rapidly than others, and catalytic effects accelerate this equilibration.

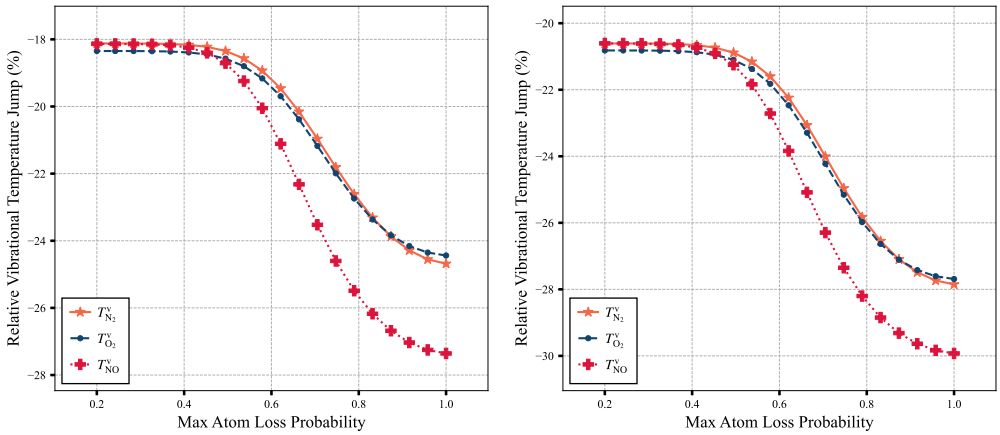

FIG. 4. Relative variations of vibrational temperatures in the $N_2/O_2/NO/N/O$ mixture; comparison of approaches to accounting for particle loss. Wall temperature $T^{w} = 1000$ K (left); $T^{w} = 500$ K (right); vibrational temperatures $T^{v} = 2000$ K.

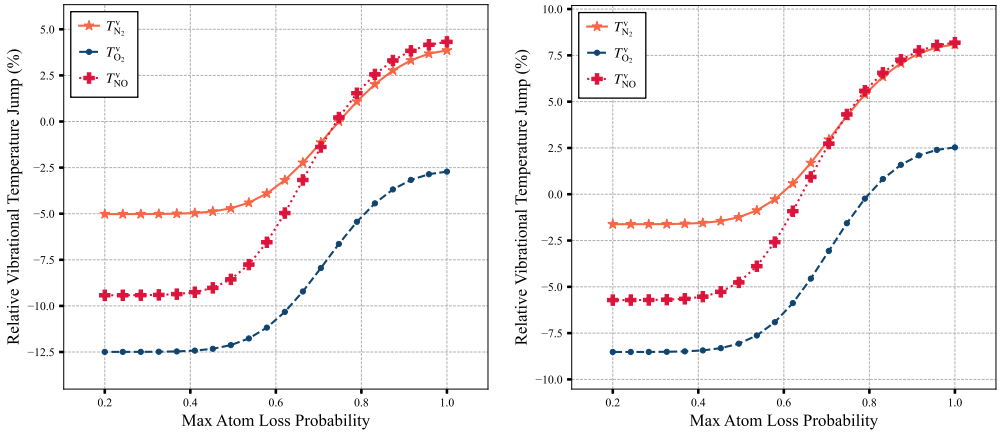

FIG. 5. Relative variations of vibrational temperatures in the $N_2/O_2/NO/N/O$ mixture; comparison of approaches to accounting for particle loss. Wall temperature $T^{w} = 1000$ K (left); $T^{w} = 500$ K (right); vibrational temperatures $T^{v} = 700$ K.

In contrast, when the wall temperature is lower than the initial vibrational temperature, the vibrational temperature tends to approach the temperature jump value for low catalyticity, while at high catalyticity, it tends toward the wall temperature (this effect is primarily observed when the difference between the gas-phase vibrational and wall temperatures is significant).

The figures show how significantly the vibrational temperatures can change and how the surface contributes to equilibration, indicating that vibrational temperature jumps make substantial contributions and must be taken into account.

D. Rotational energy accommodation

The next step is to evaluate the influence of rotational energy accommodation within each approach. The results for the five-component air mixture, considering the same gas-phase macroscopic parameter values and the same accommodation coefficients as in the previous section, are presented in Fig. 6. These figures also include separate curves for the relative temperature when diffusion effects are neglected. Neglecting diffusion results in temperature jumps that are inde-

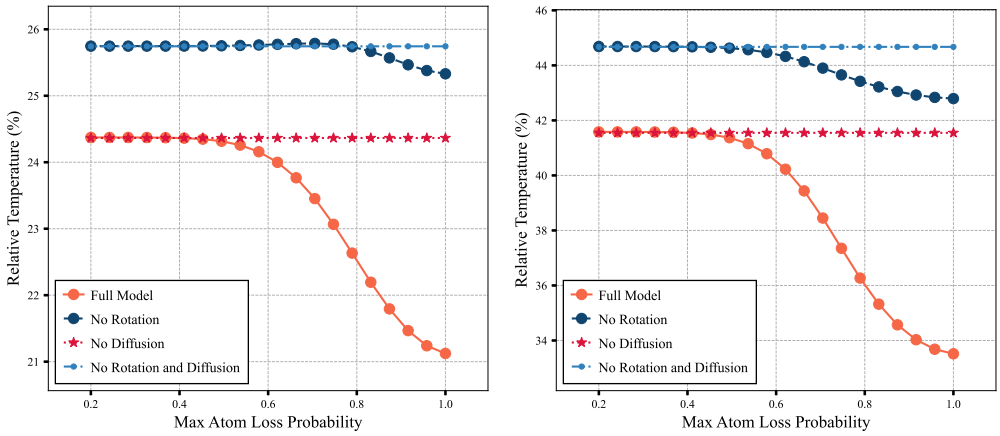

FIG. 6. Relative temperature variation ΔT as a function of maximum recombination probability in $N_2/O_2/NO/N/O$ mixture; effects of diffusion and rotational energy accommodation. Wall temperature: $T^w = 1000$ K (left); $T^w = 500$ K (right).

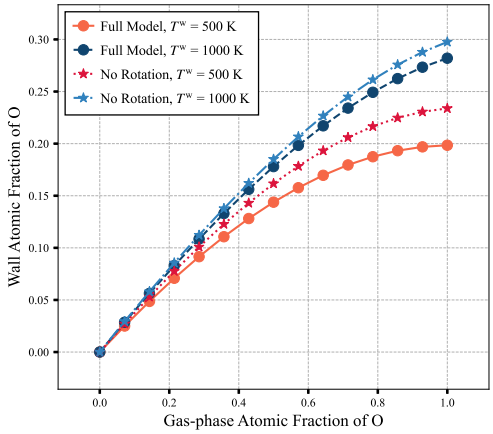

FIG. 7. Dependence of the molar fraction of atomic oxygen in the O_2/O mixture on the initial concentration; fully-catalytic wall.

pendent of γ (the same conclusion can also be drawn for vibrational TJs). Neglecting the rotational relaxation leads to a systematic increase in the temperature jump.

Figure 6 shows that when rotational energy accommodation is neglected, the temperature jump decreases with increasing recombination probability. However, this decrease is very small, almost similar to the case when both rotation effects and diffusion effects are neglected in the temperature jump. The effect of rotational relaxation on the temperature jump is about 2–4% for small values of γ and 5–15% for high values. The difference arises due to the dependence of recombination rates on the temperature jump and the gap between the gas-phase and wall temperatures. It should also be noted that the mixture composition affects the results, and the assessed contributions are valid only for the chosen composition and the accommodation coefficients. In general, the higher the molecular fractions, the stronger the effect of rotational energy accommodation, as discussed below. The impact of rotational relaxation on the vibrational temperatures is rather small, for the considered cases the differences are within 1-2%.

The influence of the models under variation of the initial atomic concentration is also of interest. The corresponding

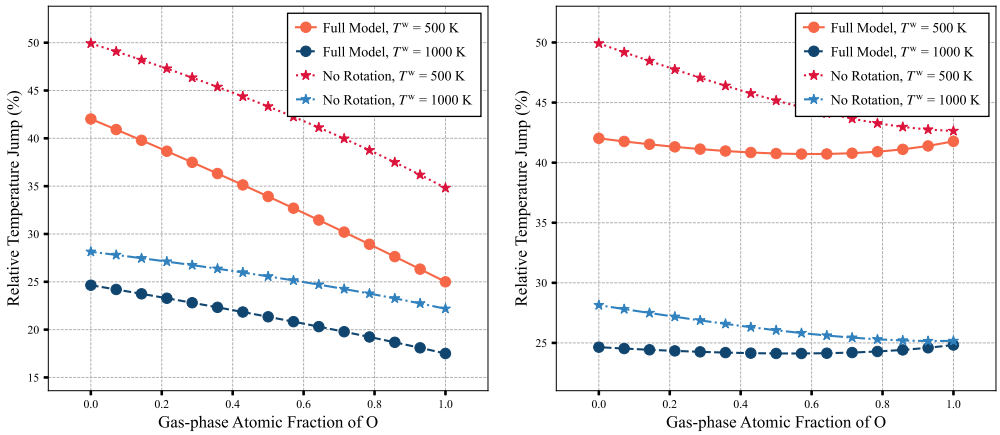

FIG. 8. Dependence of the temperature jump in the O_2/O mixture on the initial concentration; fully-catalytic wall (left); partially catalytic wall with $\gamma \approx 0.5$ (right).

results for the O_2/O mixture are presented in Fig.7 (molar fractions, fully-catalytic wall) and Fig.8 (temperature jump, fully catalytic and partially catalytic wall cases). The differences in molar fractions are primarily due to variations in the temperature jump, with noticeable deviations observed at high initial atom concentrations. At lower recombination probabilities, the differences remain small. In addition, the effect of temperature jump when catalytic properties are fixed is also confirmed: the smaller the temperature jump, the greater the impact of heterogeneous recombination.

All the obtained results indicate the necessity of including rotational relaxation, especially for mixtures with large molecular fractions. These findings are relevant not only for slip boundary condition models but also for kinetic approaches, where these effects must also be taken into account.

E. Total heat fluxes

In this section we examine the impact of rotational, vibrational relaxation and diffusion on the total heat flux near the surface (14). The five-component air mixture is considered with the same gas-phase macroparameters, and the wall temperature set to 1000 K. The results are presented in Fig. 9.

In particular, in Figure 9, we consider two separate cases: with and without vibrational temperature jumps. As can be seen, the impact of vibrational energy relaxation is quite significant, especially for high recombination probabilities and in the case of an initially strongly non-equilibrium gas flow, with the vibrational temperature much greater than the wall temperature. When vibrational temperature jumps are not considered, the total heat flux is lower in absolute values. Correct evaluation of vibrational temperatures near the wall leads to a higher heat flux to the surface.

Neglecting rotational relaxation as well leads to a smaller absolute value of the heat flux when recombination probabilities are small, and to a much larger value when the surface is almost fully catalytic. In conclusion, the effects of internal energy relaxation are significant when gas-flow temperatures differ from the surface temperature, and must be incorporated into the boundary conditions for correct evaluation of the surface heat flux.

Diffusion has no significant impact on the heat flux for low values of γ. Thus, when only heat flux evaluation is required, and the surface has low catalyticity, diffusion effects can be neglected, and the heat flux can be estimated based on the obtained temperature jumps values.

F. Knudsen number effects in slip BCs

Finally, we study the dependence of the obtained slip boundary conditions on pressure and, consequently, on Knudsen number variations. The gas-phase macroparameters are the same as in the previous sections, except for pressure, which is varied. We analyze the impact of the Knudsen number using the five-component air mixture and set the wall temperature to 1000 K. The influence of the Knudsen number on molar fractions and temperature jump is shown in Fig. 10.

The results show a common behavior for both molar fractions and temperature jump: the higher the Kn number, the stronger the rarefaction effects, the larger the TJ, and the smaller the impact of wall catalyticity. The molar fractions, represented by nitrogen molecules, are strongly affected by pressure variations, but the difference is significant only for high γ values. The variations in concentration can exceed 100% for $\gamma > 0.5$, while for smaller recombination probabilities the effects are less pronounced. For small γ, the dif-

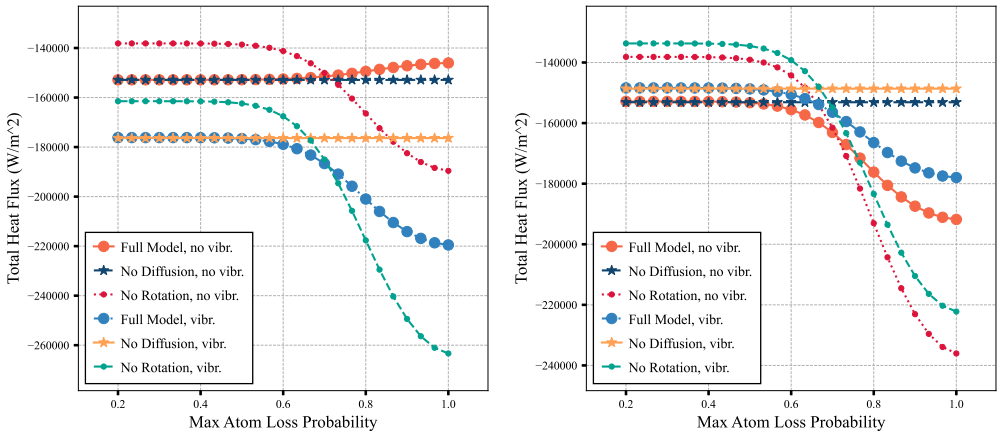

FIG. 9. Total heat fluxes in the $N_2/O_2/NO/N/O$ mixture; influence of various processes. Wall temperature $T^w = 1000$ K; vibrational temperatures $T^v = 2000$ K (left); $T^v = 700$ K (right).

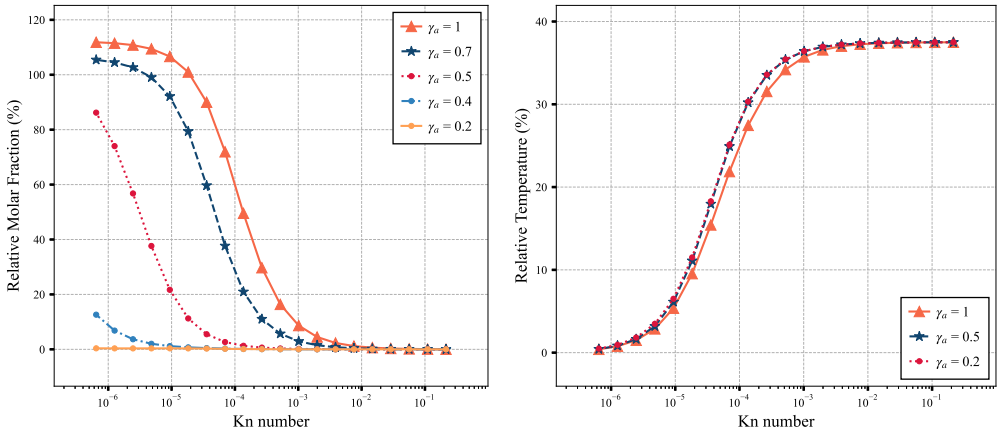

FIG. 10. Influence of the Knudsen number on changes in the distribution of nitrogen molecules and temperature jumps in the $N_2/O_2/NO/N/O$ mixture. Wall temperature $T^w = 1000$ K.

ferences for denser gases are about 1–2%. The temperature jump, as expected, decreases at higher pressures. The variations in the temperature near the surface with recombination probabilities are small and almost negligible (1) in the high-pressure case, since the temperature jump itself is small; and (2) in the upper range of Knudsen numbers, where, as can be seen from the molar fraction plots, the impact of surface catalyticity is limited due to gas rarefaction.

The total heat flux is directly connected with the dependence on the Knudsen number observed for the molar fractions and temperature jumps (see Fig.11). The absolute values of the heat flux monotonically increase with increasing pressure. For gas flows in the slip regime (Kn$>$ 0.001), their values are small, and the impact of recombination probability is minimal. In contrast, for very small Knudsen numbers, corresponding to the continuum limit, the impact of recombination probability is much more significant. In this case, the inclusion of heterogeneous reactions leads to smaller flux values. This is related to how the mixture composition affects the thermal conductivity coefficients, which, in turn, influence the

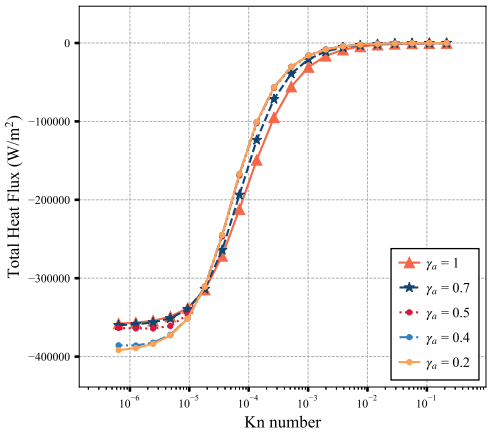

FIG. 11. Influence of the Knudsen number on the total heat flux in the $N_2/O_2/NO/N/O$ mixture. Wall temperature $T^w = 1000$ K.

heat flux values under high pressure conditions.

VI. CONCLUSIONS

In this work, we formulated a theoretical method for obtaining a closed set of slip boundary conditions in the frame of a multitemperature reacting mixture flow description. The method is based on the kinetic boundary condition and was developed by adjusting the method developed previously for the state-to-state flow model. Additionally, we proposed a new approach for accounting for the loss of gas species that participate in the formation of other species or are adsorbed.

Applying the developed method and considering two approaches for the particle loss, we derived boundary conditions for the multitemperature set of fluid dynamic variables, which include species concentrations, velocity, translational-rotational temperature, and vibrational temperatures defined for each molecular species in the mixture. This set of slip boundary conditions simultaneously accounts for rarefaction effects in gas mixture flows near the surface, the particles scattering model, and heterogeneous reactions. In this work, we derived the slip BCs specifically for the specular-diffusive scattering model.

The vibrational temperature jumps within the detailed multitemperature mixture flow description, without any additional phenomenological assumptions, have been obtained for the first time. The derived relations describe how vibrational temperatures change under the chosen scattering model and heterogeneous processes. In this work, we formulated the relations for a simplified description of vibrational relaxation due to surface scattering, assuming that diffusely scattered particles have vibrational temperatures equal to the wall temperature. However, more physically realistic models can also be implemented within the developed framework.

Using a simplified formulation of the obtained slip boundary conditions, where velocity slip is neglected and only heterogeneous recombination among surface processes is considered, we developed a solver that calculates the BCs as a solution to a nonlinear system of equations for an arbitrary gas mixture of atoms and diatomic molecules. Recommendations for implementing these slip BCs are also provided.

A parametric study of how different models and processes affect the values of macroscopic parameters near the wall has also been performed. In this study, we investigated how the particle loss model, rotational relaxation due to molecule–wall collisions (for the first time considered in the slip boundary conditions), and surface recombination influence the macroscopic parameters and heat fluxes. The developed particle loss model provides much more physically consistent results than the one previously used in our studies. As for rotational relaxation, its impact is quite significant and should be incorporated into the temperature jump formulation to enable accurate evaluation of the heat fluxes near the surface. The vibrational temperature jumps must be taken into account since their impact on the heat flux is also rather significant. Besides that, without properly implemented boundary conditions for vibrational temperatures, the effects of vibrational relaxation due to species scattering and heterogeneous reactions are not taken into account, leading to an inaccurate description of mixture flows near the surface.

The effects of heterogeneous recombination are significant mainly for high values of the recombination probability, when approaching the fully-catalytic wall case. For small recombination probabilities, $\gamma < 0.5$, the influence is practically negligible. However, it should be noted that although some effects may appear negligible in a parametric study, these small variations may have a significant impact on gas flow parameters when solving time-dependent or spatially inhomogeneous

problems. For example, small variations in mass fractions near the wall due to heterogeneous recombination can have a considerable impact on the heat flux.

To summarize, the slip boundary condition models developed in this study are capable of capturing many of non-equilibrium effects that occur when a non-equilibrium gas mixture flow interacts with a solid wall. In the future work, we plan to extend the models to polyatomic gas mixtures, investigate the influence of diffusion models, and develop simplified versions that can be directly implemented into fluid dynamic solvers.

SUPPLEMENTARY MATERIAL

Some derivation steps for the obtained slip boundary conditions, along with the necessary simplifications, are provided in the Supplementary Material.

ACKNOWLEDGMENTS

This study was supported by the Ministry of Science and Higher Education of the Russian Federation, project No. 075-15-2024-544.

AUTHOR DECLARATIONS

Conflict of Interest

The authors have no conflicts of interest to disclose.

Author Contributions

Liia Shakurova: Conceptualization, Methodology, Formal Analysis, Writing/Review & Editing, Software, Verification, **Elena Kustova:** Methodology, Formal Analysis, Writing/Review & Editing, Funding Acquisition.

DATA AVAILABILITY STATEMENT

The data that support the findings of this study are available from the corresponding author upon reasonable request.

REFERENCES

[1]C. Park, *Nonequilibrium Hypersonic Aerothermodynamics* (J.Wiley and Sons, New York, Chichester, Brisbane, Toronto, Singapore, 1990).
[2]E. Nagnibeda and E. Kustova, *Nonequilibrium Reacting Gas Flows. Kinetic Theory of Transport and Relaxation Processes* (Springer Verlag, Berlin, Heidelberg, 2009).
[3]M. Capitelli, D. Bruno, and A. Laricchiuta, *Fundamental Aspects of Plasma Chemical Physics: Transport*, Springer Series on Atomic, Optical, and Plasma Physics, Vol. 74 (Springer Verlag, Berlin, 2013).
[4]I. D. Boyd and T. E. Schwartzentruber, *Nonequilibrium Gas Dynamics and Molecular Simulation*, Cambridge Aerospace Series (Cambridge University Press, Cambridge, New York, 2017).
[5]G. V. Candler, "Rate effects in hypersonic flows," Annual Review of Fluid Mechanics **51**, 379–402 (2019).
[6]L. Pietanza, O. Guaitella, V. Aquilanti, I. Armenise, A. Bogaerts, M. Capitelli, G. Colonna, V. Guerra, R. Engeln, E. Kustova, A. Lombardi, F. Palazzetti, and T. Silva, "Advances in non-equilibrium CO_2 plasma kinetics: a theoretical and experimental review," European Physical Journal D **75** (2021), 10.1140/epjd/s10053-021-00226-0.
[7]G. A. Bird, *Molecular Gas Dynamics and the Direct Simulation of Gas Flows* (Clarendon, Oxford, England, UK, 1994).
[8]M. S. Ivanov and S. F. Gimelshein, "Computational hypersonic rarefied flows," Annual Review of Fluid Mechanics **30**, 469–505 (1998).
[9]S. Chapman and T. G. Cowling, *The mathematical theory of non-uniform gases: an account of the kinetic theory of viscosity, thermal conduction and diffusion in gases* (Cambridge university press, 1990).
[10]J. O. Hirschfelder, C. F. Curtiss, and R. B. Bird, *Molecular theory of gases and liquids* (New York: Wiley, 1964).
[11]W. G. Vincenti, C. H. Kruger Jr, and T. Teichmann, *Introduction to physical gas dynamics* (American Institute of Physics, 1966).
[12]E. Kustova and E. Nagnibeda, "Transport properties of a reacting gas mixture with strong vibrational and chemical nonequilibrium," Chem. Phys. **233**, 57–75 (1998).
[13]M. Capitelli, C. Ferreira, B. Gordiets, and A. Osipov, *Plasma Kinetics in Atmospheric Gases*, Springer series on atomic, optical and plasma physics, Vol. 31 (Springer-Verlag, Berlin, 2000).
[14]M. Panesi, A. Munafò, T. E. Magin, and R. L. Jaffe, "Nonequilibrium shock-heated nitrogen flows using a rovibrational state-to-state method," Phys. Rev. E **90**, 013009 (2014).
[15]C. O. Johnston and M. Panesi, "Impact of state-specific flowfield modeling on atomic nitrogen radiation," Phys. Rev. Fluids **3**, 013402 (2018).
[16]S. F. Gimelshein, I. J. Wysong, A. J. Fangman, D. A. Andrienko, O. V. Kunova, E. V. Kustova, C. Garbacz, M. Fossati, and K. Hanquist, "Kinetic and continuum modeling of high-temperature oxygen and nitrogen binary mixtures," Journal of Thermophysics and Heat Transfer **36**, 399–418 (2022).
[17]D. Ninni, F. Bonelli, G. Colonna, and G. Pascazio, "Unsteady behavior and thermochemical non equilibrium effects in hypersonic double-wedge flows," Acta Astronautica **191**, 178–192 (2022).
[18]D. Ninni, F. Bonelli, G. Colonna, and G. Pascazio, "On the influence of non equilibrium in the free stream conditions of high enthalpy oxygen flows around a double-cone," Acta Astronautica **201**, 247–258 (2022).
[19]X. Wang, J. Guo, Q. Hong, and S. Li, "High-fidelity state-to-state modeling of hypersonic flow over a double cone," Physics of Fluids **35**, 116101 (2023).
[20]C. Park, "Chemical-kinetic problems of future NASA missions. I. Earth entries," J. Thermophys. Heat Transfer **7**, 385–398 (1993).
[21]C. Park, J. Howe, R. Howe, R. Jaffe, and G. Candler, "Review of chemical-kinetic problems of future NASA missions, II: Mars entries," J. Thermophys. Heat Transfer **8**, 9–23 (1994).
[22]A. Chikhaoui, J. Dudon, E. Kustova, and E. Nagnibeda, "Transport properties in reacting mixture of polyatomic gases," Physica A **247**, 526–552 (1997).
[23]A. Chikhaoui, J. Dudon, S. Genieys, E. Kustova, and E. Nagnibeda, "Multitemperature kinetic model for heat transfer in reacting gas mixture," Physics of Fluids **12**, 220–232 (2000).
[24]E. Kustova and G. Oblapenko, "Reaction and internal energy relaxation rates in viscous thermochemically non-equilibrium gas flows," Phys. Fluids **27**, 016102 (2015).
[25]E. Kustova and G. Oblapenko, "Mutual effect of vibrational relaxation and chemical reactions in viscous multitemperature flows," Phys. Rev. E **93**, 033127 (2016).
[26]A. Kosareva, O. Kunova, E. Kustova, and E. Nagnibeda, "Four-temperature kinetic model for CO_2 vibrational relaxation," Physics of Fluids **33**, 016103 (2021).
[27]A. Kosareva, O. Kunova, E. Kustova, and E. Nagnibeda, "Hybrid approach to accurate modeling of coupled vibrational-chemical kinetics in carbon dioxide," Physics of Fluids **34**, 026105 (2022).

[28]L. Shakurova, I. Armenise, and E. Kustova, "State-specific slip boundary conditions in non-equilibrium gas flows: Theoretical models and their assessment," Physics of Fluids **35**, 086109 (2023).
[29]F. Sharipov and V. Seleznev, "Data on internal rarefied gas flows," Journal of Physical and Chemical Reference Data **27**, 657–706 (1998).
[30]F. Sharipov, "Data on the velocity slip and temperature jump on a gas–solid interface," Journal of Physical and Chemical Reference Data **40**, 023101 (2011).
[31]O. Teixeira, D. Santos, and J. Azevedo, "Catalytic wall effects for hypersonic nozzle flow in nonequilibrium conditions," Acta Astronautica **205**, 468–478 (2023).
[32]I. Nompelis, G. V. Candler, and M. S. Holden, "Effect of vibrational nonequilibrium on hypersonic double-cone experiments," AIAA journal **41**, 2162–2169 (2003).
[33]F. Bonelli, M. L. Facchini, F. Nasuti, and G. Colonna, "Effect of finite-rate catalysis on wall heat flux prediction in hypersonic flow," Physical Review Fluids **6**, 033201 (2021).
[34]S. Zhang and Z. Wang, "Effects of chemical energy accommodation on nonequilibrium flow and heat transfer to a catalytic wall," Chinese Journal of Aeronautics **35**, 165–175 (2022).
[35]K. S. Gopalan and coauthors, "Development of a detailed surface chemistry framework in SPARTA (SurfChem)," Computer Physics Communications (2025), 10.1016/j.cpc.2025.109263, implementation of catalytic surface chemistry for DSMC.
[36]M. Larini and R. Brun, "Wall temperature jumps in non-equilibrium polyatomic gases," International Journal of Heat and Mass Transfer **16**, 2189–2203 (1973).
[37]T. Gökçen, R. MacCormack, and D. Chapman, "Computational fluid dynamics near the continuum limit," AIAA Paper , 987–1115 (1987).
[38]J. Meloans, I. Graur, A. Ketsdever, and E. Muntz, "New thermal conditions at the wall in high speed flows," in *Rarefied Gas Dynamics, 23rd International Symposium*, Vol. 663 (2003) pp. on CD–ROM.
[39]B. A. Kiryutin and G. Tirskiy, "Slip boundary conditions on a catalytic wall in a chemically reacting multicomponent many-temperature gas flow with excited internal degrees of freedom of particles," in *Hypersonic Aerodynamics and Heat Transfer* (Begell House, 2013).
[40]S. Kosuge, K. Aoki, M. Bisi, M. Groppi, and G. Martalò, "Boundary conditions for two-temperature Navier-Stokes equations for a polyatomic gas," Physical Review Fluids **6**, 083401 (2021).
[41]A. Kumar and A. S. Rana, "H-theorem and boundary conditions for two-temperature model: Application to wave propagation and heat transfer in polyatomic gases," Physical Review E **108**, 065103 (2023).
[42]H. Liu, Q. Li, W. Chen, and L. Wu, "On the shock wave boundary layer interaction in slightly rarefied gas," Physics of Fluids **36** (2024).
[43]L. Shakurova and E. Kustova, "State-specific boundary conditions for nonequilibrium gas flows in slip regime," Phys. Rev. E **105**, 034126 (2022).
[44]L. Shakurova and E. Kustova, "Slip boundary conditions for gas mixture flows with state-to-state vibrational-chemical kinetics," *32nd International Symposium on Rarefied Gas Dynamics*, AIP Conference Proceedings **2996**, 130002 (2024).
[45]E. Kustova and D. Giordano, "Cross-coupling effects in chemically non-equilibrium viscous compressible flows," Chem. Phys. **379**, 83–91 (2011).
[46]C. Cercignani, "Scattering kernels for gas-surface interactions," Transport Theor. Stat. Ph. **2**, 27–53 (1972).
[47]S. Nocilla, "Basic concepts in the surface interaction of free-molecular flows or molecular beams," Meccanica **2**, 34–40 (1967).
[48]C. Cercignani and M. Lampis, "Kinetic models for gas-surface interactions," Transport Theor. Stat. Ph. **1**, 101–114 (1971).
[49]C. Scott, "Wall boundary equations with slip and catalysis for multicomponent, nonequilibrium gas flows," NASA TM X-58111 (1973).
[50]M. Epstein, "A model of the wall boundary condition in kinetic theory," AIAA J. **5**, 1797–1800 (1967).
[51]K. Aoki and V. Giovangigli, "Kinetic theory of chemical reactions on crystal surfaces," Phys. A: Stat. Mech. Appl. **565**, 125573 (2021).
[52]R. K. Hanson, "Experimental study of shock-wave reflection from a thermally accommodating wall," The Physics of Fluids **16**, 369–374 (1973).
[53]O. Tumuklu, D. A. Levin, and V. Theofilis, "Investigation of unsteady, hypersonic, laminar separated flows over a double cone geometry using a kinetic approach," Physics of Fluids **30** (2018).
[54]P. Valentini, M. S. Grover, A. M. Verhoff, and N. J. Bisek, "Near-continuum, hypersonic oxygen flow over a double cone simulated by direct simulation Monte Carlo informed from quantum chemistry," Journal of Fluid Mechanics **966**, A32 (2023).
[55]A. Kroupnov and M. J. Pogosbekian, "Interaction of dissociated air with the surface of β-cristobalite material," Acta Astronautica **203**, 454–468 (2023).
[56]J. Breen, D. Rosner, W. Delgass, P. Nordine, R. Cibrian, and N. Krishnan, "Catalysis study for space shuttle vehicle thermal protection systems," Tech. Rep. (Yale University, 1973).
[57]C. Scott, "Catalytic recombination of nitrogen and oxygen on high-temperature reusable surface insulation," in *15th Thermophysics Conference* (1980) p. 1477.
[58]V. Berkut, V. Doroshenko, V. Kovtun, N. Koudryavtsev, S. Novikov, N. Smirnov, and A. Sharotovov, "Measurements of the probability of the heterogeneous atom recombination on heated surfaces in a supersonic flow," Soviet Journal of Chemical Physics **9**, 2222–2237 (1992).
[59]M. Balat-Pichelin, J. Badie, R. Berjoan, and P. Boubert, "Recombination coefficient of atomic oxygen on ceramic materials under earth re-entry conditions by optical emission spectroscopy," Chemical Physics **291**, 181–194 (2003).
[60]A. N. Molchanova, A. V. Kashkovsky, and Y. A. Bondar, "Surface recombination in the direct simulation Monte Carlo method," Physics of Fluids **30**, 107105 (2018).
[61]P. Kolodziej and D. Stewart, "Nitrogen recombination on high-temperature reusable surface insulation and the analysis of its effect on surface catalysis," in *22nd Thermophysics Conference* (1987) p. 1637.
[62]W. Seward and E. Jumper, "Model for oxygen recombination on silicon-dioxide surfaces," Journal of thermophysics and heat transfer **5**, 284–291 (1991).
[63]O. Deutschmann, U. Riedel, and J. Warnatz, "Modeling of nitrogen and oxygen recombination on partial catalytic surfaces," ASME. J. Heat Transfer **117**, 495–501 (1995).
[64]T. Kurotaki, T. Ito, K. Ishida, and T. Matsuzaki, "CFD evaluation of pressure effects on surface catalysis of SiO_2-based TPS," in *43rd AIAA Aerospace Sciences Meeting and Exhibit* (2005) p. 388.
[65]F. Nasuti, M. Barbato, and C. Bruno, "Material-dependent recombination modeling for hypersonic flows," J. Thermophys. Heat Transfer **10**, 131–136 (1996).
[66]M. Barbato, S. Reggiani, C. Bruno, and J. Muylaert, "Model for heterogeneous catalysis on metal surfaces with applications to hypersonic flows," Journal of Thermophysics and Heat Transfer **14**, 412–420 (2000).
[67]M. Rutigliano and M. Cacciatore, "Eley–Rideal recombination of hydrogen atoms on a tungsten surface," Physical Chemistry Chemical Physics **13**, 7475–7484 (2011).
[68]M. Rutigliano and M. Cacciatore, "Recombination of oxygen atoms on silica surface: new and more accurate results," Journal of Thermophysics and Heat Transfer **30**, 247–250 (2016).
[69]A. Kroupnov and M. J. Pogosbekian, "Adsorption of oxygen and nitrogen atoms on the SiO_2 surface: Molecular dynamics calculation based on the quantum-mechanical potential," Fluid Dynamics **59**, 924–931 (2024).
[70]L. Shakurova, I. Armenise, and E. Kustova, "Effect of slip boundary conditions on nonequilibrium reacting air flows," Journal of Theoretical and Applied Mechanics, Sofia **53**, 253–269 (2023).
[71]M. Norkin, L. Shakurova, and E. Kustova, "Numerical solution to Couette problem for monatomic gas flow in slip regime," Vestnik St. Petersburg University, Mathematics **58**, 289–298 (2025).